JCAMECH

Nonlinear analytical solution of nearly incompressible hyperelastic cylinder with variable thickness under non-uniform pressure by perturbation technique

Hamed Gharooni and Mehdi Ghannad[*]

Department of Mechanical Engineering, Shahrood University of Technology, Shahrood, Iran,

---

ARTICLE INFO

ABSTRACT

In this paper, nonlinear analytical solution of pressurized thick cylindrical shells with variable thickness made of hyperelastic materials is presented. The governing equilibrium equations for the cylindrical shell with variable thickness under non-uniform internal pressure are derived based on first-order shear deformation theory (FSDT). The shell is assumed to be made of isotropic and homogenous hyperelastic material in nearly incompressible condition. Two-term Mooney-Rivlin type material is considered which is a suitable hyperelastic model for rubbers. Boundary Layer Method of the perturbation theory which is known as Match Asymptotic Expansion (MAE) is used for solving the governing equations. In order to validate the results of the current analytical solution in analyzing pressurized hyperelastic thick cylinder with variable thickness, a numerical solution based on Finite Element Method (FEM) have been investigated. Afterwards, for a rubber case study, displacements, stresses and hydrostatic pressure distribution resulting from MAE and FEM solution have been presented. Furthermore, the effects of geometry, loading, material properties and incompressibility parameter have been studied. Considering the applicability of the rubber elasticity theory to aortic soft tissues such as elastin, the behaviour of blood vessels under non-uniform pressure distribution has been investigated. The results prove the effectiveness of FSDT and MAE combination to derive and solve the governing equations of nonlinear problems such as nearly incompressible hyperelastic shells.

---

1. Introduction

Hyperelastic materials are quite common in many engineering applications. In the last decades, many constitutive models are developed for hyperelastic materials, which can be used in computational model according to the application. The Mooney-Rivlin model of hyperelastic materials can simulate most of the mechanical behaviour of the rubber materials. The model provides a good description of the mechanical properties of rubber materials when deformation is less than 150% [1]. Rubber products are used in different industrial applications; such as rubber hose to carry fluids, rubber anti-vibration mountings, cylindrical pneumatic floating rubber fenders for boats and so on. Furthermore, rubber seals for sealing connectors are used to very easily seal on the internal or the external diameters of test parts which have smooth cylindrical connections. Rubber cylindrical sleeves have been used for many years successfully for label printing and have been proven of value for the established printing processes. The Mooney-Rivlin model of rubber materials completely satisfies the performance calculation of packer rubber materials. When the packer rubber supports pressure from a liquid, it experiences a relatively large deformation, which produces a larger contact pressure and forms a seal between the rubber and the casing, resulting in sealing of the annular gap and isolation of the production layer. The load capacity of the packer rubber is a function of the contact pressure that exists during the sealing process [2]. These materials are incompressible or

almost incompressible and undergo large strains when subjected to loads. Nevertheless, computational modelling poses challenges owing to incompressibility. For example, the displacement based finite element methods, which are widely used for various applications and materials, are not efficient for almost incompressible materials. Sussman and Bathe [3] introduce a displacement-pressure (u/p) finite element formulation for the geometrically and materially nonlinear analysis of compressible and almost incompressible solids. An important research on "slightly compressible" concept was developed by LevinsonI and Burgesse in 1971 [4]. Simo and Taylor [5] in 1982 analyzed incompressible nonlinear elastic solids by a penalty function approach. They investigated the formulation and numerical analysis of constitutive equations for finite elasticity in terms of principal stretches in 1991 [6]. Chen and their assistants [7] presented a pressure projection method for the nonlinear analysis of structures made of nearly incompressible hyperelastic materials in 1996. The main focus of their second part of the paper was to demonstrate the performance of the previous method and to address some of the issues related to the analysis of engineering elastomers including the proper selection of strain energy density functions [8]. Bijelonja et al. [9] presented development of a displacement-pressure based finite volume formulation for modelling of large strain problems involving incompressible hyperelastic materials. The incompressibility constraint is enforced by employing the integral form of the mass

---

[*] Corresponding author: *Ghannad.mehdi@gmail.com*

conservation equation in deformed configurations of the body and a Mooney–Rivlin incompressible material model is used for material description. Silva and Bittencourt [10] presented shape optimization of nearly incompressible hyperelastic structural problems for the Mooney-Rivlin hyperelastic model. Doll and Schweizerhof [11] reviewed the isochoric-volumetric decoupling of the strain energy function. Ghaemi et al. [12] developed a compressible pseudo-strain energy function that describes the mechanical behaviour of rubber-like materials. Montella et al. [13] presented the mechanical behaviour of a Tire Derived Material in details. A hyper elastic material law for silicones has been developed and validated by Dias et al. [14] based on a strain energy function.

The problem of the finite axisymmetric deformation of a thick-walled circular cylindrical elastic tube subjected to pressure on the external lateral boundaries was formulated for an incompressible isotropic neo-Hookean material by Zhu et al. [15]. Tanveer and Zu [16] presented finite amplitude transient vibration analysis of nearly incompressible hyperelastic axisymmetric solids by a mixed p-type method which displacement and pressure fields were separately defined using high degree polynomials and the solution was obtained with one or a few elements depending upon the nature of the problem. Kiendl et al. [17] presented formulations for compressible and incompressible hyperelastic thin shells with plane stress condition based on energy methods.

In optimizing a shell with respect to weight or stress distribution, one method is to use shells with varying thickness or material properties. The literature that addresses the stresses of thick cylindrical shells with variable thickness is quite limited. Eipakchi [18] calculated stresses and displacements of linear elastic conical shell with varying thickness under non-uniform internal pressure analytically, using third-order shear deformation theory. Ghannad et al. [19] presented a closed-form analytical solution for clamped-clamped thick cylindrical shells with variable thickness made of functionally graded materials subjected to constant internal pressure based on the first-order shear deformation theory. Jabbari et al. [20] presented semi-analytical solution of rotating truncated conical shells with varying thickness made of functionally graded materials (FGMs) subjected to thermo-mechanical loading. The system of partial differential equations is semi-analytically solved by using multi-layered method (MLM). Gharooni and Ghannad investigated thermo-elastic analysis in pressurized thick FGM cylinders with varying properties of power function based on higher-order shear deformation theory [21].

Significant manifestation of cardiovascular disease involves a regional dilation of the aorta termed an aortic aneurysm (AA) which is a focal dilatation of the aortic wall. The decision to surgically intervene prior to AA rupture is made with recognition of significant procedural risks, and is primarily based on the maximal diameter and/or growth rate of the AA. Therefore, a pressing need remains to identify better predictors of rupture risk and ultimately integrate their measurement into clinical decision making and evaluate the relative sensitivity of wall stress to geometrical and mechanical properties of the aneurysmal tissue. In pathologic conditions, arteries are even under more shear deformation compared to healthy vessels. For example, atherosclerosis and calcification are typically, localized, therefore, certain portions of the wall are hardened in contrast to the rest of the wall. Under pulsatile action, the normal portion of the wall can naturally stretch

considerably while the diseased portions may not be able to stretch as much and, therefore, shearing may occur at the boundary between the diseased and healthy portions of the wall. In clinical interventions, such as balloon angioplasty and balloon embolectomy significant wall shearing may take place. In vessel transplantation, shear deformation is important. For example in using mammary or femoral vessel for a coronary bypass, the straight vessel must be bent to match the curvature of coronary vessel in which it is subjected to shear deformation [22]. In analysis such as finite element method or shear deformation theory, simulation of arterial tissues under blood pressure could result in useful information. In 1968, Thomas et al. [23] studied incompressibility condition to the analysis of arterial-wall elasticity. They concluded that for most practical purposes arteries may be considered nearly incompressible. The applicability of the rubber elasticity theory to elastin has been tested by Dorrington and McCrum [24] for simple tension of a homogeneous rubber. They proved that elastin is not a normal elastomer but conforms to a new model, termed the liquid drop elastomer and review the earlier experiments in which elastin was shown to conform more or less to the theory of rubber elasticity. Mihai and Goriely [25] investigated the fact that the physical responses of nonlinear elastic materials are generally described by parameters which are scalar functions of the deformation, and their particular choice is not always clear. Reference [26] is a very useful book which covers the fundamentals of biomechanics and topics including biosolids, biofluids, stress, balance and equilibrium. Various biological parameters (for instance mean blood vessel characteristics) are presented in this book. Azar et al. [27] used a series of finite element-based computational models that represent a range of plausible aortic aneurysm scenarios, and evaluated the relative sensitivity of wall stress to geometrical and mechanical properties of the aneurysmal tissue.

Most of the studies reviewed investigate that analytical solution of pressurized hyperelastic thick cylindrical shells with variable thickness has not been studied in the literature. On the other hand, most of the previous studies have not acceptable results because of failing to take into account shear stresses or the displacement based finite element methods which are not efficient for almost incompressible materials. The common problems with these methods, when Poisson's ratio approaches 0.5, are the incorrect displacements and stresses, the ill conditioning of stiffness matrix, and the locking phenomena. Furthermore, investigating aortic aneurysm as pressurized hyperelastic blood vessels enable scientists to evaluate the relative sensitivity of displacement and stress to geometrical and mechanical properties of the aneurysmal tissue. In order to improve the approximation and take into account the effect of shear stresses and strains, the general method of derivation and nonlinear analysis of hyperelastic thick-walled cylindrical shells with variable thickness under non-uniform internal pressure has been presented in this paper by using FSDT. The hyperelastic material of the shell is assumed to be isotropic and homogeneous with two-term Mooney-Rivlin material description in nearly incompressible condition. The extension of incompressible materials to nearly incompressible materials is considered. Two ends of thick-walled vessel have clamped boundary conditions. The variation of pressure and thickness are along axial direction of the shell. Because of fast convergence, closed form solution and compatibility with physics of shell, Boundary Layer Method of

the perturbation theory which is known as Match Asymptotic Expansion (MAE) is used for solving the governing equations. A new ingenious formulation and parameters have been defined during current study to simplify and abbreviate the representation of inner and outer equations components in MAE. In addition, the terms of variable thickness and non-uniform pressure have been presented in special representation. Displacements, stresses and hydrostatic pressure distribution resulting from MAE solution have been presented for some case studies and the results have been compared with a FE modeling in ANSYS software. Current study aims to illustrate the performance of the potentials and their reliability for the prediction of the state of deformation and stress in hyperelastic vessels from rubbers to arteries. We present the equations that provide the general continuum description of the deformation and the hyperelastic stress response of the material. The present study takes advantage of the FSDT and MAE combination in order to identify the elastic behaviour of the pressurized rubber-like shells, human aneurismal aortic tissues and the stresses of critical points at failure under common pressure of blood vessels. We will discuss the constituents of arterial walls from the mechanical perspective and emphasize those aspects which are important to researchers interested in constitutive issues.

2. Basic formulations

2.1. Shear deformation theory

In this study, we consider a thick-walled cylindrical shell with variable thickness under non-uniform internal pressure (Fig. 1). In the reference configuration, geometry based on the terms of cylindrical polar coordinate is:

$$r_i \leq r \leq r_o(x), \quad 0 \leq \theta \leq 2\pi, \quad 0 \leq x \leq L \tag{1}$$

where r_i and $r_o(x)$, respectively, are the inner and outer radius and L is the length of the shell. The parameter r is the radius of every layer of cylinder in the reference configuration which can be replaced in terms of radius of mid-plane $R(x)$ and distance of every layer with respect to mid-plane (z):

$$r = R(x) + z,$$

$$-\frac{h(x)}{2} \leq z \leq \frac{h(x)}{2} \Rightarrow dr = dz, \tag{2}$$

$$(r, \theta, x) \Rightarrow (z, \theta, x)$$

$h(x)$ is the thickness of the cylinder which is varying along axial direction. The following relations can be written for the geometry components of the shell:

$$R(x) = r_i + \frac{h(x)}{2},$$

$$r_o(x) = r_i + h(x), \tag{3}$$

$$h(x) = h_a - \left(\frac{h_a - h_b}{L}\right)x$$
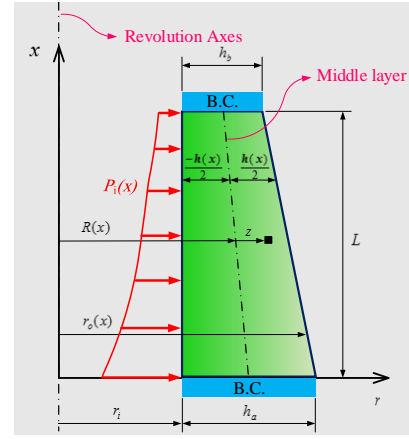
Figure 1. Geometry and B.C. of the cylindrical shell with variable thickness under non-uniform internal pressure

The general axisymmetric displacement field, in the first-order Mirsky-Hermann's theory could be expressed on the basis of radial displacement U_z and axial displacement U_x, as follows

$$U_z(z, x) = w(x) + z\psi(x),$$

$$U_\theta = 0, \tag{4}$$

$$U_x(z, x) = u(x) + z\varphi(x)$$

where $w(x)$ and $u(x)$ are the displacement components of the middle surface. Also, $\psi(x)$ and $\varphi(x)$ are the rotational components used to determine the displacement field.

The deformation gradient tensor $[\mathbf{F}]$ in the matrix representation has the form [15] $\left(( )' = \partial( )/\partial x\right)$

$$[\mathbf{F}] = \begin{bmatrix} 1+\psi & 0 & w'+\psi'z \\ 0 & 1+\dfrac{w+\psi z}{R+z} & 0 \\ \varphi & 0 & 1+u'+\varphi'z \end{bmatrix} \tag{5}$$

Consequently, the right Cauchy–Green deformation tensor $[\mathbf{C}] = [\mathbf{F}]^{\mathrm{T}}[\mathbf{F}]$ and its principal invariants $I_{1,2,3}$ are

$$\begin{cases} [\mathbf{C}] = \begin{bmatrix} C_{zz} & 0 & C_{zx} \\ 0 & C_{\theta\theta} & 0 \\ C_{xz} & 0 & C_{xx} \end{bmatrix}, \\[4pt] C_{zz} = (1+\psi)^2 + \varphi^2, \quad C_{\theta\theta} = \left(1+\dfrac{w+\psi z}{R+z}\right)^2 \\[4pt] C_{xx} = (w'+\psi'z)^2 + (1+u'+\varphi'z)^2, \\[4pt] C_{zx} = C_{xz} = (1+\psi)(w'+\psi'z) + \varphi(1+u'+\varphi'z) \end{cases} \tag{6}$$

$$I_1 = C_{zz} + C_{\theta\theta} + C_{xx},$$

$$I_2 = C_{zz}C_{\theta\theta} + C_{\theta\theta}C_{xx} + C_{zz}C_{xx} - C_{zx}^2, \tag{7}$$

$$I_3 = C_{zz}C_{\theta\theta}C_{xx} - C_{\theta\theta}C_{zx}^2 = J^2$$

Jacobian which is known as volume ratio of deformation has the following terms (det is determinant operator):

$$J = \det(\mathbf{F}) = \left(\frac{1}{R(x)+z}\right)$$

$$\times \left[(R(x)+z+w+\psi z)\binom{(1+\psi)(1+u'+\varphi'z)}{-\varphi(w'+\psi'z)}\right] \tag{8}$$

The Green–Lagrange strain tensor can be defined as $\mathbf{E} = 1/2(\mathbf{C}-\mathbf{I})$ ($[\mathbf{I}]$ is the identity tensor). Considering Voigt notation for Green–Lagrange strains, its components are as follows:

$$\begin{cases} \varepsilon_{zz} = \psi + \dfrac{\psi^2}{2} + \dfrac{\varphi^2}{2}, \\[2mm] \varepsilon_{xx} = u' + \dfrac{u'^2}{2} + \dfrac{w'^2}{2} + \left(\varphi' + u'\varphi' + w'\psi'\right)z + \left(\dfrac{\varphi'^2}{2} + \dfrac{\psi'^2}{2}\right)z^2 \\[2mm] \varepsilon_{\theta\theta} = \dfrac{w+\psi z}{R(x)+z} + \dfrac{(w+\psi z)^2}{2(R(x)+z)^2}, \\[2mm] \gamma_{zx} = 2\varepsilon_{zx} = \varphi + u'\varphi + w' + w'\psi + \left(\psi' + \psi\psi' + \varphi\varphi'\right)z \end{cases} \quad (9)$$

2.2. Hyperelastic material constitutive equation

Based on the assumption of isotropy, the strain energy density function depends either on the left or the right Cauchy–Green deformation tensor through the strain invariants $(W(I_1, I_2, I_3))$. If the material is modeled as incompressible, the determinant of deformation gradient is equal to unity $(J=1)$. For incompressible models, under homogenous deformation, two of the invariants of Cauchy–Green deformation gradient vary independently. Conversely, if the material is defined as compressible, all the invariants are independent and the determinant of the Cauchy–Green deformation gradient (J) is the measure of the local volume change during deformation. In this study, the proposed strain energy function was developed based on the invariants I_1, I_2 and J.

In the present case, the extension of incompressible materials to nearly incompressible materials is considered; means that the incompressibility constraint is replaced with a penalty function correspond to the constraint. The strain energy function for nearly incompressible materials can be decomposed into isochoric and volumetric part using the deformation invariants and the volume change (Jacobian) as [5]:

$$W(I_1, I_2, J) = \hat{W}(I_1, I_2, J) + \tilde{W}(J) \quad (10)$$

where $\hat{W}$ and $\tilde{W}$ are the isochoric and the volumetric part of strain energy function, respectively. We can write

$$\hat{W}(I_1, I_2, J) = W^*(I_1, I_2) + cH(J) \quad (11)$$

$$\tilde{W}(J) = \frac{1}{2}\lambda\{G(J)\}^2 \quad (12)$$

W^* is the response of the material to distortional part of the deformation in Eq. (15). In the present study, a two-term Mooney-Rivlin type material is considered. It has the following form [1]:

$$W^*(I_1, I_2) = C_1(I_1-3) + C_2(I_2-3) \quad (13)$$

where C_1 and C_2 are material constants resulting from experimental tests.

$G(J)$ in Eq. (12) is a penalty function which has to satisfy the conditions $G(J) = 0 \Leftrightarrow J = 1$ and $\lambda > 0$ is a penalty parameter which can be estimated by experimental data proportional to the material properties and is known as compressibility parameter [28]. Therefore it is reasonable to assume that rubber is almost incompressible. This is accomplished by dropping the restriction $J=1$ and including a hydrostatic work term in the strain energy function [5]. Considering the compressibility parameter as $\lambda = k$, where k is an additional material constant representing the bulk modulus, only scales the penalty functions but does not change their shapes [12]. In this case, k is the ratio of the volumetric stress (hydrostatic pressure (P)) to the volumetric strain [23,25].

$$k = \frac{P}{\Delta V/V} = \frac{P}{J-1} \quad (14)$$

V_0 and ΔV are the reference volume and volume changes through deformation, respectively. For the volumetric part, there are many forms proposed by researchers which are functions of bulk modulus and the Jacobian [5,6,29]. Generally, in the limiting state, the volumetric part of the strain energy function has to satisfy the condition $J \to 1 \Rightarrow \tilde{W}(J) \to 1, \tilde{W}'(J) \to 0, \tilde{W}''(J) \to k$.

Considering zero values of displacement components in the reference configurations (initial state) with Eqs. (5), (6) and (7) lead in $[\mathbf{F}]=[\mathbf{C}]=[\mathbf{I}]$ and $(I_1, I_2, I_3, J) = (3,3,1,1)$. In the second term of the right hand side of Eq. (11), constant c and function $H(J)$ with the condition $H(J) = 0, H'(J) = 1 \Leftrightarrow J = 1$ only guarantee the stress free reference configuration with no physical meaning. Moreover, in the general case of nearly incompressible hyperelasticity (as Mooney-Rivlin material), hydrostatic pressure $P = k(J-1)$ does not vanish even at the natural state. The first condition $(H(J) = 0)$ corresponds to the incompressibility constraint $J = 1$ and the second condition $(H'(J) = 1)$ is necessary for giving the meaning of pressure to the constant multiplier of H as $c = -p_0$. Then the initial value of P (i.e. p_0), which has no clear physical meaning, must be introduced to make the initial stress zero [5].

In the current study, the function $H(J)$ and $G(J)$ are considered as [5,30]

$$H(J) = \ln(J), \qquad G(J) = J-1 \quad (15)$$

Finally, the strain energy per unit undeformed volume of a two-term Mooney–Rivlin material model in nearly incompressible condition and coupled form is expressed by [5,10,30]

$$W = C_1(I_1-3) + C_2(I_2-3) - p_0\ln(J) + \frac{k}{2}(J-1)^2 \quad (16)$$

Consequently, constitutive equation of coupled Mooney-Rivlin model in material description and nearly incompressible, isotropic and homogenous conditions would result [30,31].

$$\mathbf{S} = 2\frac{\partial W(I_1, I_2, J)}{\partial \mathbf{C}} \quad (17)$$
$$= 2[C_1 + C_2 I_1]\mathbf{I} - 2C_2\mathbf{C} + [kJ(J-1) - p_0]\mathbf{C}^{-1}$$

C_1, C_2 and k are material constants and $[\mathbf{I}]$ is the identity tensor. The initial stress is zero if the hydrostatic pressure vanishes at the natural state, and vice versa. Recalling the assumption of stress-free reference configuration, Eq. (17)

result in $p_0 = 2(C_1 + 2C_2)$ [5,9]. Thus, the multiplier p_0 in the case of $H(J) = \ln(J)$ denotes the pressure measured in the initial volume. The other components in the right hand side of Eq. (17) can be written in the displacement field components. Therefore, the relation between the second Piola–Kirchhoff stress tensor and displacement components could be derived.

2.3. Principle of virtual work

The basic idea of the principle of virtual work is to couple kinematically admissible virtual deformations with force variables and stresses of the real deformation process. For convenience, we suppose that the boundary surface A_0 of the body consists of two parts $A_{0\mathbf{y}}$ and $A_{0\sigma}$ where displacements $\mathbf{y}$ and forces $\mathbf{t}_0$ are prescribed, respectively. Based on the principle of virtual work, the variation of strain energy of the elastic body is equal to the variation of external work due to loading [17,31,32].

$$\delta\Pi = \delta\Pi_{\text{EXT}} - \delta\Pi_{\text{INT}} = 0$$
$$= \iiint_{V_0} \delta\mathbf{y} \cdot (\rho_0 \mathbf{b}_0 - \rho_0 \mathbf{a}) dV_0 + \iint_{A_{0\sigma}} \delta\mathbf{y} \cdot \mathbf{t}_0 dA_0 - \iiint_{V_0} \mathbf{P} : \delta\mathbf{F} dV_0 \quad (18)$$

where ρ_0, V_0 and $\mathbf{b}_0$ are density, volume and body force in undeformed configuration, respectively. $\mathbf{a}$ is dynamic acceleration. $[\mathbf{P}]$ and $[\mathbf{F}]$ are first Piola–Kirchhoff stress and deformation gradient tensors, respectively. Kinematically admissible virtual deformation variables are understood to be the variations $\delta\mathbf{y}$ and $\delta\mathbf{F}$ which are subjected to the constraints (GRAD is gradient operator)

$$\delta\mathbf{F} = \text{GRAD}\,\delta\mathbf{y} \quad \text{in } V_0, \qquad \delta\mathbf{y} = 0 \quad \text{on } A_{0\mathbf{y}} \quad (19)$$

Therefore, the principle of virtual work (Eq. (18)) is a weak formulation of the equations of motion as well as the dynamic boundary conditions. Equality of energy conjugate variables preserves its validity as $\mathbf{P} : \delta\mathbf{F} = \mathbf{S} : \delta\mathbf{E}$. In the static equilibrium and absence of body forces, Eq. (18) results in the variation of external work consists of non-uniform internal pressure $P_i(x)$ applying at the internal surface A_i of cylinder:

$$\delta\Pi_{\text{EXT}} = \iint_{A_0} \delta\mathbf{y} \cdot \mathbf{t}_0 \, dA_0 = \iint_{A_i} P_i(x) \delta U_z \big|_{r=r_i} \, dA_i,$$
$$dA_i = 2\pi r_i \, dx \quad (20)$$

Considering displacement components from Eq. (4), we can rewrite Eq. (20):

$$\delta\Pi_{\text{EXT}} = \int_0^L 2\pi P_i(x) \left(R(x) - \frac{h(x)}{2} \right) \left(\delta w - \frac{h(x)}{2} \delta\psi \right) dx \quad (21)$$

The internal virtual work in material description can be expressed from Eq. (18) and energy conjugate variables

$$\delta\Pi_{\text{INT}} = \iiint_{V_0} \mathbf{S} : \delta\mathbf{E} dV_0 = \iiint_{V_0} S^{ij} \delta\varepsilon_{ij} dV_0,$$
$$dV_0 = 2\pi r(x) dr \, dx = 2\pi (R(x) + z) dz \, dx \quad (22)$$

Considering Voigt notation from Eq. (9), the variation of strain energy of cylinder with variable thickness can be derived based on non-zero physical components of second Piola–Kirchhoff stress:

$$\delta\Pi_{\text{INT}} = 2\pi \int_0^L \int_{-h(x)/2}^{+h(x)/2} \left[\begin{array}{l} S^{zz} \delta\varepsilon_{zz} + \\ S^{\theta\theta} \delta\varepsilon_{\theta\theta} + \\ S^{xx} \delta\varepsilon_{xx} + S^{zx} \delta\gamma_{zx} \end{array} \right] R(x) \left(1 + \frac{z}{R(x)} \right) dz \, dx \quad (23)$$

The stress resultants are defined as follows:

$$\{ N_z \quad M_z \quad Q_z \}^{\text{T}} = \int_{-h(x)/2}^{+h(x)/2} S^{zz} \{ 1 \quad z \quad z^2 \}^{\text{T}} \left(1 + \frac{z}{R(x)} \right) dz \quad (24)$$

$$\{ N_\theta \quad M_\theta \quad Q_\theta \}^{\text{T}} = \int_{-h(x)/2}^{+h(x)/2} S^{\theta\theta} \{ 1 \quad z \quad z^2 \}^{\text{T}} dz \quad (25)$$

$$\{ \bar{N}_\theta \quad \bar{M}_\theta \quad \bar{Q}_\theta \}^{\text{T}} = \int_{-h(x)/2}^{+h(x)/2} S^{\theta\theta} \{ 1 \quad z \quad z^2 \}^{\text{T}} \left(\frac{R(x)}{R(x) + z} \right) dz \quad (26)$$

$$\{ N_x \quad M_x \quad Q_x \}^{\text{T}} = \int_{-h(x)/2}^{+h(x)/2} S^{xx} \{ 1 \quad z \quad z^2 \}^{\text{T}} \left(1 + \frac{z}{R(x)} \right) dz \quad (27)$$

$$\{ N_{zx} \quad M_{zx} \quad Q_{zx} \}^{\text{T}} = K_S \int_{-h(x)/2}^{+h(x)/2} S^{zx} \{ 1 \quad z \quad z^2 \}^{\text{T}} \left(1 + \frac{z}{R(x)} \right) dz \quad (28)$$

In the last equation, K_S is shear correction factor which is applying in the stress resultant derived from shear stresses because of preventing stress overestimation. We consider $K_S = 5/6$ in the present study [19,33].

Calculating strain invariants from Eq. (9) and substituting results into Eqs. (23) and (21), considering $\delta\Pi_{\text{EXT}} = \delta\Pi_{\text{INT}}$ and carrying out the integration by parts, the equilibrium equations for the cylindrical shell with variable thickness under non-uniform internal pressure are obtained in the term of stress resultants:

$$\frac{d}{dx} \left[R(x) \left(N_x (1 + u') + M_x \varphi' + N_{zx} \varphi \right) \right] = 0 \quad (29)$$

$$\frac{d}{dx} \left[R(x) \left(M_x (1 + u') + Q_x \varphi' + M_{zx} \varphi \right) \right]$$
$$- R(x) \left(N_z \varphi + N_{zx} (1 + u') + M_{zx} \varphi' \right) = 0 \quad (30)$$

$$\frac{d}{dx} \left[R(x) \left(N_x w' + M_x \psi' + N_{zx} (1 + \psi) \right) \right]$$
$$- N_\theta - \frac{1}{R(x)} \left(\bar{N}_\theta w + \bar{M}_\theta \psi \right) = -P_i(x) \left(R(x) - \frac{h(x)}{2} \right) \quad (31)$$

$$\frac{d}{dx} \left[R(x) \left(M_x w' + Q_x \psi' + M_{zx} (1 + \psi) \right) \right] - M_\theta$$
$$- R(x) \left(N_z (1 + \psi) + N_{zx} w' + M_{zx} \psi' \right)$$
$$- \frac{1}{R(x)} \left(\bar{M}_\theta w + \bar{Q}_\theta \psi \right) = P_i(x) \frac{h(x)}{2} \left(R(x) - \frac{h(x)}{2} \right) \quad (32)$$

3. Analytical solution

3.1. Perturbation theory

In this article, Boundary Layer Method of the perturbation theory which is known as Match Asymptotic Expansion (MAE) is used for solving the governing equations. The advantages of this method are fast convergence, closed form solution and compatibility with physics of shell. MAE can explain the behaviour of the shell successfully even near the boundaries. The governing equations (29)-(32) for cylinder with variable thickness is a system of four nonlinear coupled differential equations with variable coefficients. Preliminary definitions,

simplifications and preparations are necessary for using MAE. At first, it is necessary to convert the equations into dimensionless form for making use of the characteristic scales. The following dimensionless parameters are defined [18,34]:

$$\bar{x}=\frac{x}{L}, \quad \bar{h}=\frac{h}{h_0}, \quad \bar{z}=\frac{z}{h_0}, \quad \bar{r}_i=\frac{r_i}{h_0}, \quad \bar{R}=\frac{R}{h_0}, \quad \bar{u}=\frac{u}{h_0}, \quad \bar{\varphi}=\varphi, \quad \bar{w}=\frac{w}{h_0}, \quad (33)$$

The mark $^{-}$ on the parameters denotes the dimensionless quantity. h_0 is the characteristic thickness which is commonly consider the smallest thickness in shell. ε is perturbation parameter which is assumed small quantity. The main idea of perturbation theory is that perturbation parameter is so small that coefficients of different power of it don't have the same order which is lead in equality for ε^i coefficients. Considering each coefficient result in displacement quasi vector $\{\bar{\mathbf{y}}(\bar{x})\}$. Existence of two boundary layer lead in two region of solution near boundaries (inner expansions) and a solution away from boundaries (outer expansion) [34].

In the dimensionless forms, first and second order differential based on $\bar{x}$ should be rewrite as follows:

$$\frac{\mathrm{d}}{\mathrm{d}x}=\frac{1}{L}\frac{\mathrm{d}}{\mathrm{d}\bar{x}}, \quad \frac{\mathrm{d}^2}{\mathrm{d}x^2}=\frac{1}{L^2}\frac{\mathrm{d}^2}{\mathrm{d}\bar{x}^2} \quad (34)$$

In shear deformation theory, the differentials and integrations are with respect to $\bar{x}$ and $\bar{z}$, respectively. Therefore, for simplification and abbreviation of representing equations, a dimensionless integral is defined:

$$\overline{II}(\mathrm{i},\mathrm{j})=\frac{II(\mathrm{i},\mathrm{j})}{h_0^{\mathrm{i}+\mathrm{j}+1}}=\int_{-\bar{h}(\bar{x})/2}^{+\bar{h}(\bar{x})/2}\bar{z}^{\mathrm{i}}\left(\bar{R}(\bar{x})+\bar{z}\right)^{\mathrm{j}}\mathrm{d}\bar{z} \quad (35)$$

which is the function of geometric parameters $\bar{R}(\bar{x})$ and $\bar{h}(\bar{x})$. In order to solve the set of governing differential equations, the inverse of coefficient matrices (defined in the next sections) are needed. To do this, we take integrate the first equation in the set of Eqs. (29)-(32). The constant of integral is $\bar{c}_0=c_0/\varepsilon$ where ε is bookkeeping perturbed parameter. As there is no $\bar{u}$ in equations unlike $\mathrm{d}\bar{u}/\mathrm{d}\bar{x}$, we take $\bar{v}=\mathrm{d}\bar{u}/\mathrm{d}\bar{x}$. Therefore, we can write $\bar{u}=\int\bar{v}\,\mathrm{d}\bar{x}+c_7$ where c_7 is integral constant. $\bar{c}_0$ and c_7 will be calculated from boundary conditions.

The following parameters need to be defined based on material and geometrical constants C_1,C_2,k,K_s because of abbreviation in representing inner and outer equations.

$$\begin{cases} 2(C_1+C_2)=C_{12},\, (1-K_s)=\hat{K}_s,\, 4(C_1+C_2)-k=Ck_1, \\ 4(C_1+2C_2)-k=Ck_2, 2(C_1+C_2)-3k=Ck_3, \\ 2(C_1+C_2)-k=Ck_4,\, 4(C_1+C_2)-5k=Ck_5, \\ 4(C_1+C_2)-6k=Ck_6,\, 8(C_1+2C_2)-7k=Ck_7, \\ 2(2C_1+3C_2)-k=Ck_8,\, 2(2C_1+5C_2)-6k=Ck_9 \end{cases} \quad (36)$$

3.2. Outer expansion

The outer expansion of solution is considered as a uniform series of ε as $\bar{\mathbf{y}}_O(\bar{x},\varepsilon)=\varepsilon\left(\bar{\mathbf{y}}_{O0}(\bar{x})+\varepsilon\bar{\mathbf{y}}_{O1}(\bar{x})\right)$. Substituting of this expansion in governing equations and considering the terms with the same order of ε, result in the first and second

order equations of outer solution. In this section $(\ )'=\mathrm{d}(\ )/\mathrm{d}\bar{x}$.

$$O(\varepsilon^1):[\mathbf{A}_O]\{\bar{\mathbf{y}}_{O0}\}=\{\mathbf{F}_{O0}\},$$
$$O(\varepsilon^2):[\mathbf{A}_O]\{\bar{\mathbf{y}}_{O1}\}=\{\mathbf{F}_{O1}^{\mathrm{t}}\}, \quad (37)$$
$$\{\mathbf{F}_{O1}^{\mathrm{t}}\}=\{\mathbf{F}_{O1}^{II}\}+\{\mathbf{F}_{O1}^{II'}\}$$

where $[\mathbf{A}_O],\{\mathbf{F}_{O0}\}$ and $\{\mathbf{F}_{O1}^{\mathrm{t}}\}$ are coefficient matrices, non-homogeneity vectors of first and second order equation, respectively. $\{\bar{\mathbf{y}}_{Oi}\}$ are unknown displacement vectors in (i) order outer solution. $\{\mathbf{F}_{O1}^{\mathrm{t}}\}$ consist of two vectors $\{\mathbf{F}_{O1}^{II}\}$ and $\{\mathbf{F}_{O1}^{II'}\}$ correspond with $\overline{II}(\bar{x})$ and derivative of $\overline{II}(\bar{x})$, respectively. These vectors would be defined in appendices. Other nonzero components of the mentioned matrix and vectors are

$$\{\bar{\mathbf{y}}_{O0}\}=\{\bar{v}_{O0},\bar{\varphi}_{O0},\bar{w}_{O0},\bar{\psi}_{O0}\}^{\mathrm{T}},$$
$$\{\bar{\mathbf{y}}_{O1}\}=\{\bar{v}_{O1},\bar{\varphi}_{O1},\bar{w}_{O1},\bar{\psi}_{O1}\}^{\mathrm{T}} \quad (38)$$

$$\begin{cases} [\mathbf{A}_O]_{11}=k\,\overline{II}(0,1), \quad [\mathbf{A}_O]_{22}=-K_sC_{12}\overline{II}(0,1), \\ [\mathbf{A}_O]_{13}=-[\mathbf{A}_O]_{31}=-Ck_1\overline{II}(0,0) \\ [\mathbf{A}_O]_{14}=-[\mathbf{A}_O]_{41}=-Ck_1\left(\overline{II}(1,0)+\overline{II}(0,1)\right), \\ [\mathbf{A}_O]_{33}=-k\,\overline{II}(0,-1) \\ [\mathbf{A}_O]_{34}=[\mathbf{A}_O]_{43}=Ck_1\overline{II}(0,0)-k\,\overline{II}(1,-1), \\ [\mathbf{A}_O]_{44}=2Ck_1\overline{II}(1,0)-k\left(\overline{II}(0,1)+\overline{II}(2,-1)\right) \end{cases} \quad (39)$$

$$\{\mathbf{F}_{O0}\}_1=\frac{\bar{c}_0}{h_0^2}, \quad \{\mathbf{F}_{O0}\}_2=0,$$
$$\{\mathbf{F}_{O0}\}_3=-\bar{P}_i(\bar{x})\left(\bar{R}(\bar{x})-\frac{\bar{h}(\bar{x})}{2}\right), \quad (40)$$
$$\{\mathbf{F}_{O0}\}_4=\bar{P}_i(\bar{x})\left(\frac{\bar{R}(\bar{x})\bar{h}(\bar{x})}{2}-\frac{\bar{h}^2(\bar{x})}{4}\right)$$

The solutions of the algebraic equations (48) are as follows:
$$\{\bar{\mathbf{y}}_{O0}\}=[\mathbf{A}_O]^{-1}\{\mathbf{F}_{O0}\}, \quad \{\bar{\mathbf{y}}_{O1}\}=[\mathbf{A}_O]^{-1}\{\mathbf{F}_{O1}^{\mathrm{t}}\} \quad (41)$$

3.3. Inner expansion

As the outer solutions don't satisfy the B.C., we can conclude existence of boundary layers at $\bar{x}=0,1$. Therefore, it should be considered fast variables ($\tilde{x}_\alpha$) as a new variables for these regions. Considering fast variables make it possible to measure the great variation around boundaries.

$$\bar{x}=0\rightarrow\alpha=0,\quad \tilde{x}_0=\frac{\bar{x}}{\varepsilon} \quad \text{(left boundary)},$$
$$\bar{x}=1\rightarrow\alpha=1,\quad \tilde{x}_1=\frac{(\bar{x}-1)}{\varepsilon} \quad \text{(right boundary)} \quad (42)$$

New first and second order differential definitions based on fast variables $\tilde{x}_\alpha$ have perturbation parameter:

$$\frac{\mathrm{d}}{\mathrm{d}\tilde{x}_\alpha}=\varepsilon\frac{\mathrm{d}}{\mathrm{d}\bar{x}}, \quad \frac{\mathrm{d}^2}{\mathrm{d}\tilde{x}_\alpha^2}=\varepsilon^2\frac{\mathrm{d}^2}{\mathrm{d}\bar{x}^2} \quad (43)$$

In cylinder with variable thickness and non-uniform pressure, it is necessary to derive Taylor expansion for all the parameters of axial function $\bar{\Lambda}(\bar{x})$:

$$\begin{cases} \bar{\Lambda}(\bar{x}) = \bar{\Lambda}(\bar{x}=\alpha) + (\bar{x}-\alpha)\dfrac{\mathrm{d}\,\bar{\Lambda}(\bar{x})}{\mathrm{d}\,\bar{x}}\bigg|_{\bar{x}=\alpha} , \quad (\alpha=0,1) \\ \bar{\Lambda}(\tilde{x}) = \bar{\Lambda}_{\alpha} + \varepsilon\tilde{x}_{\alpha}\mathrm{D}\bar{\Lambda}_{\alpha}, \quad (\alpha=0,1) \end{cases} \quad (44)$$

Subscript index $(\ )_{\alpha}$ means applying $\bar{x}=\alpha$ in each parameter. Therefore, we should write Taylor expansion for the following parameters:

$$\begin{cases} \bar{h}(\tilde{x}) = \bar{h}_{\alpha} + \varepsilon\tilde{x}_{\alpha}\mathrm{D}\bar{h}_{\alpha}, \quad (\alpha=0,1), \\ \bar{R}(\tilde{x}) = \bar{R}_{\alpha} + \varepsilon\tilde{x}_{\alpha}\mathrm{D}\bar{R}_{\alpha}, \quad (\alpha=0,1), \\ \bar{P}_{\mathrm{i}}(\tilde{x}) = \bar{P}_{i\alpha} + \varepsilon\tilde{x}_{\alpha}\mathrm{D}\bar{P}_{i\alpha}, \quad (\alpha=0,1), \\ \overline{\mathit{\Pi}}_{\alpha}(\tilde{x}) = \overline{\mathit{\Pi}}_{\alpha} + \varepsilon\tilde{x}_{\alpha}\mathrm{D}\overline{\mathit{\Pi}}_{\alpha}, \quad (\alpha=0,1) \end{cases} \quad (45)$$

The inner expansion of solution is considered as a uniform series of ε in each boundary:

$$\bar{\mathbf{y}}_{\alpha}(\tilde{x}_{\alpha},\varepsilon) = \varepsilon\left(\bar{\mathbf{y}}_{\alpha0}(\tilde{x}_{\alpha}) + \varepsilon\bar{\mathbf{y}}_{\alpha1}(\tilde{x}_{\alpha})\right) \quad (46)$$

Substituting of inner expansion $\bar{\mathbf{y}}_{\alpha}(\tilde{x}_{\alpha},\varepsilon) = \varepsilon\left(\bar{\mathbf{y}}_{\alpha0}(\tilde{x}_{\alpha}) + \varepsilon\bar{\mathbf{y}}_{\alpha1}(\tilde{x}_{\alpha})\right)$ in governing equations with mentioned changes in section 3.1 and considering terms with the same order of ε, result in inner equations at boundary α :

$$\begin{cases} \mathrm{O}(\varepsilon^1): [\mathbf{A}_{\alpha1}]\dfrac{\mathrm{d}^2}{\mathrm{d}\,\tilde{x}_{\alpha}^{\,2}}\{\bar{\mathbf{y}}_{\alpha0}\} + [\mathbf{A}_{\alpha2}]\dfrac{\mathrm{d}}{\mathrm{d}\,\tilde{x}_{\alpha}}\{\bar{\mathbf{y}}_{\alpha0}\} + [\mathbf{A}_{\alpha3}]\{\bar{\mathbf{y}}_{\alpha0}\} = \{\mathbf{F}_{\alpha0}\} \\ \mathrm{O}(\varepsilon^2): [\mathbf{A}_{\alpha1}]\dfrac{\mathrm{d}^2}{\mathrm{d}\,\tilde{x}_{\alpha}^{\,2}}\{\bar{\mathbf{y}}_{\alpha1}\} + [\mathbf{A}_{\alpha2}]\dfrac{\mathrm{d}}{\mathrm{d}\,\tilde{x}_{\alpha}}\{\bar{\mathbf{y}}_{\alpha1}\} + [\mathbf{A}_{\alpha3}]\{\bar{\mathbf{y}}_{\alpha1}\} = \{\mathbf{F}_{\alpha1}^{\mathrm{t}}\} \\ \{\mathbf{F}_{\alpha1}^{\mathrm{t}}\} = \{\mathbf{F}_{\alpha1}^{\mathit{\Pi}\alpha}\} + \{\mathbf{F}_{\alpha1}^{\mathrm{D}A\alpha}\} + \{\mathbf{F}_{\alpha1}^{\mathrm{D}\mathit{\Pi}\alpha}\} + \{\mathbf{F}_{\alpha1}^{P\alpha}\} + \{\mathbf{F}_{\alpha1}^{\mathrm{D}P\alpha}\} \end{cases} \quad (47)$$

$[\mathbf{A}_{\alpha1}], [\mathbf{A}_{\alpha2}]$ and $[\mathbf{A}_{\alpha3}]$ are coefficient matrices at the boundary α . $\{\mathbf{F}_{\alpha0}\}$ and $\{\mathbf{F}_{\alpha1}^{\mathrm{t}}\}$ are non-homogeneity vectors of differential equation at the $\mathrm{O}(\varepsilon^1)$ and $\mathrm{O}(\varepsilon^2)$ for the boundary α , respectively. $\{\bar{\mathbf{y}}_{\alpha\mathrm{i}}\}$ are unknown displacement vectors in (i) th order of inner solution at the boundary α . $\{\mathbf{F}_{\alpha1}^{\mathit{\Pi}\alpha}\}$ and $\{\mathbf{F}_{\alpha1}^{\mathrm{D}\mathit{\Pi}\alpha}\}$, in $\{\mathbf{F}_{\alpha1}^{\mathrm{t}}\}$, are correspond with $\overline{\mathit{\Pi}}_{\alpha}(\tilde{x})$ and $\mathrm{D}\overline{\mathit{\Pi}}_{\alpha}(\tilde{x})$ (in Taylor expansion), respectively. $\{\mathbf{F}_{\alpha1}^{\mathrm{D}A\alpha}\}$ occurs in non-homogeneity of $\mathrm{O}(\varepsilon^2)$ equation which resulting from Tayler expansion of coefficient matrices in $\mathrm{O}(\varepsilon^1)$ equation because of variable thickness. $\{\mathbf{F}_{\alpha1}^{P\alpha}\}$ and $\{\mathbf{F}_{\alpha1}^{\mathrm{D}P\alpha}\}$ include $\bar{P}_{i\alpha}(\tilde{x}_{\alpha})$ and $\mathrm{D}\bar{P}_{i\alpha}(\tilde{x}_{\alpha})$ (in Taylor expansion), respectively. Furthermore, $\{\mathbf{F}_{\alpha1}^{P\alpha}\}$ and $\{\mathbf{F}_{\alpha1}^{\mathrm{D}P\alpha}\}$ are resulting from variable thickness and non-uniform pressure, respectively. Considering too many terms, $\{\mathbf{F}_{\alpha1}^{\mathrm{t}}\}$ vector would be defined in appendices. Other nonzero components of the matrices and vectors defined below. In this section $(\ )' = \mathrm{d}(\ )/\mathrm{d}\tilde{x}_{\alpha}$ at the boundary α .

$$\{\bar{\mathbf{y}}_{\alpha0}\} = \{\bar{v}_{\alpha0}, \bar{\varphi}_{\alpha0}, \bar{w}_{\alpha0}, \bar{\psi}_{\alpha0}\}^{\mathrm{T}},$$
$$\{\bar{\mathbf{y}}_{\alpha1}\} = \{\bar{v}_{\alpha1}, \bar{\varphi}_{\alpha1}, \bar{w}_{\alpha1}, \bar{\psi}_{\alpha1}\}^{\mathrm{T}} \quad (48)$$

$$\begin{cases} [\mathbf{A}_{\alpha1}]_{22} = k\,\overline{\mathit{\Pi}}_{\alpha}(2,1), \\ [\mathbf{A}_{\alpha1}]_{33} = K_s C_{12}\overline{\mathit{\Pi}}_{\alpha}(0,1) \\ [\mathbf{A}_{\alpha1}]_{34} = [\mathbf{A}_{\alpha1}]_{43} = K_s C_{12}\overline{\mathit{\Pi}}_{\alpha}(1,1), \\ [\mathbf{A}_{\alpha1}]_{44} = K_s C_{12}\overline{\mathit{\Pi}}_{\alpha}(2,1) \end{cases} \quad (49)$$

$$\begin{cases} [\mathbf{A}_{\alpha2}]_{12} = [\mathbf{A}_{\alpha2}]_{21} = k\,\overline{\mathit{\Pi}}_{\alpha}(1,1), \\ [\mathbf{A}_{\alpha2}]_{23} = -[\mathbf{A}_{\alpha2}]_{32} = -K_s C_{12}\overline{\mathit{\Pi}}_{\alpha}(0,1) - Ck_1\overline{\mathit{\Pi}}_{\alpha}(1,0) \\ [\mathbf{A}_{\alpha2}]_{24} = -[\mathbf{A}_{\alpha2}]_{42} = -K_s C_{12}\overline{\mathit{\Pi}}_{\alpha}(1,1) - Ck_1\left(\overline{\mathit{\Pi}}_{\alpha}(2,0) + \overline{\mathit{\Pi}}_{\alpha}(1,1)\right) \end{cases} \quad (50)$$

$$\begin{cases} [\mathbf{A}_{\alpha3}]_{11} = k\,\overline{\mathit{\Pi}}_{\alpha}(0,1), \\ [\mathbf{A}_{\alpha3}]_{22} = -K_s C_{12}\overline{\mathit{\Pi}}_{\alpha}(0,1), \\ [\mathbf{A}_{\alpha3}]_{13} = -[\mathbf{A}_{\alpha3}]_{31} = -Ck_1\overline{\mathit{\Pi}}_{\alpha}(0,0) \\ [\mathbf{A}_{\alpha3}]_{14} = -[\mathbf{A}_{\alpha3}]_{41} = -Ck_1\left(\overline{\mathit{\Pi}}_{\alpha}(0,1) + \overline{\mathit{\Pi}}_{\alpha}(1,0)\right), \\ [\mathbf{A}_{\alpha3}]_{33} = -k\,\overline{\mathit{\Pi}}_{\alpha}(0,-1) \\ [\mathbf{A}_{\alpha3}]_{34} = [\mathbf{A}_{\alpha3}]_{43} = Ck_1\overline{\mathit{\Pi}}_{\alpha}(0,0) - k\,\overline{\mathit{\Pi}}_{\alpha}(1,-1), \\ [\mathbf{A}_{\alpha3}]_{44} = 2Ck_1\overline{\mathit{\Pi}}_{\alpha}(1,0) - k\left(\overline{\mathit{\Pi}}_{\alpha}(0,1) + \overline{\mathit{\Pi}}_{\alpha}(2,-1)\right) \end{cases} \quad (51)$$

$$\{\mathbf{F}_{\alpha0}\}_1 = \frac{\bar{c}_0}{h_0^{\,2}}, \qquad \{\mathbf{F}_{\alpha0}\}_2 = 0,$$

$$\{\mathbf{F}_{\alpha0}\}_3 = -\bar{P}_{i\alpha}\left(\bar{R}_{\alpha} - \frac{\bar{h}_{\alpha}}{2}\right),$$

$$\{\mathbf{F}_{\alpha0}\}_4 = \bar{P}_{i\alpha}\left(\frac{\bar{R}_{\alpha}\bar{h}_{\alpha}}{2} - \frac{\bar{h}_{\alpha}^{\,2}}{4}\right) \quad (52)$$

Eqs. (47) are systems of coupled non-homogenous differential equations with constant coefficients. Each equation have general and particular solution:

$$\{\bar{\mathbf{y}}_{\alpha0}\} = \{\bar{\mathbf{y}}_{\alpha0}\}_{\mathrm{gen.}} + \{\bar{\mathbf{y}}_{\alpha0}\}_{\mathrm{par.}},$$
$$\{\bar{\mathbf{y}}_{\alpha1}\} = \{\bar{\mathbf{y}}_{\alpha1}\}_{\mathrm{gen.}} + \{\bar{\mathbf{y}}_{\alpha1}\}_{\mathrm{par.}} \quad (53)$$

Considering m_{α} and $\{V_{\alpha}\}$ as eigenvalues and eigenvectors, respectively; general solution have exponential form as $\{\bar{\mathbf{y}}_{\alpha}\}_{\mathrm{gen.}} = \{V_{\alpha}\}\mathrm{e}^{m_{\alpha}\tilde{x}_{\alpha}}$. Substituting general solution in homogenous part of Eqs. (47) and considering $\mathrm{e}^{m_{\alpha}\tilde{x}_{\alpha}} \neq 0$ lead in a nonlinear eigenvalue problem:

$$\left([\mathbf{A}_{\alpha1}]m_{\alpha}^{\,2} + [\mathbf{A}_{\alpha2}]m_{\alpha} + [\mathbf{A}_{\alpha3}]\right)\{V_{\alpha}\} = \{0\} \quad (54)$$

The necessary condition for existing the solution of Eq. (54) is zero value of the coefficient determinant which is the characteristic equation of the system. Six non-zero roots of it are the eigenvalues $(m_{\alpha\mathrm{i}})$. Substituting roots in Eq. (54) lead in corresponding eigenvectors $(V_{\alpha\mathrm{i}})$. The eigenvalues and eigenvectors are complex conjugate. Considering Van-Dyke's matching principle [34], the solution should be finite at

$\tilde{x}_\alpha \to \infty$. Therefore, in left boundary ($\alpha = 0$) eigenvalues with positive real part and in right boundary ($\alpha = 1$) eigenvalues with negative real part are omitted. So, the general solution of the boundary α is calculated.

$$\{\overline{\mathbf{y}}_{\alpha 0}\}_{\text{gen.}} = \{\overline{\mathbf{y}}_{\alpha 1}\}_{\text{gen.}} = \{\overline{\mathbf{y}}_\alpha\}_{\text{gen.}} = \sum_{i=1}^{3} c_{\alpha i} \{V_{\alpha i}\} e^{m_{\alpha i} \tilde{x}_\alpha} \qquad (55)$$

where $c_{\alpha i}$ are 3 constant for each boundary which could be calculated by the boundary condition. The particular solution of first order Eq. (47) is simply calculate by $\{\overline{\mathbf{y}}_{\alpha 0}\}_{\text{par.}} = [\mathbf{A}_{\alpha 3}]^{-1} \{\mathbf{F}_{\alpha 0}\}$. But $\{\mathbf{F}_{\alpha 1}^{t}\}$ consist of nonlinear polynomials terms, exponential terms by the same roots with characteristic equations ($e^{m_{\alpha i} \tilde{x}_\alpha}$) and exponential terms by the different roots with characteristic equations ($e^{q_{\alpha j} \tilde{x}_\alpha}$) based on $O(\varepsilon^1)$ solution. Therefore, the particular solution of $O(\varepsilon^2)$ is calculated by undetermined coefficients method as follows:

$$\begin{cases} \{\overline{\mathbf{y}}_{\alpha 1}\}_{\text{par.}} = \{\overline{\mathbf{y}}_{\alpha 1}\}_{\text{par.}}^{\text{pol.}} + \{\overline{\mathbf{y}}_{\alpha 1}\}_{\text{par.}}^{\exp(m_i).} + \{\overline{\mathbf{y}}_{\alpha 1}\}_{\text{par.}}^{\exp(q_i).}, \\ \{\overline{\mathbf{y}}_{\alpha 1}\}_{\text{par.}}^{\text{pol.}} = \{B_2\} \tilde{x}^2 + \{B_1\} \tilde{x} + \{B_0\} \\ \{\overline{\mathbf{y}}_{\alpha 1}\}_{\text{par.}}^{\exp(mi).} = \sum_i \left(\{B_2\}_{mi} \tilde{x}^2 + \{B_1\}_{mi} \tilde{x} + \{B_0\}_{mi} \right) e^{m_{\alpha i} \tilde{x}_\alpha} \\ \{\overline{\mathbf{y}}_{\alpha 1}\}_{\text{par.}}^{\exp(qj).} = \sum_j \left(\{B_2\}_{qj} \tilde{x}^2 + \{B_1\}_{qj} \tilde{x} + \{B_0\}_{qj} \right) e^{q_{\alpha j} \tilde{x}_\alpha} \end{cases} \qquad (56)$$

Substituting $\{\overline{\mathbf{y}}_{\alpha 1}\}_{\text{par.}}$ in Eq. (47) - $O(\varepsilon^2)$ would lead in undetermined coefficients $\{B_0\}$, $\{B_1\}$ and $\{B_2\}$.

3.4. Composite solution

In the MAE method, the composite solution is the summation of these three calculated solutions (one outer $\{\overline{\mathbf{y}}_O\}$ and two inner $\{\overline{\mathbf{y}}_{\alpha=0}\}$, $\{\overline{\mathbf{y}}_{\alpha=1}\}$) minus the overlapped parts of them. Outer solution at $\overline{x} \to 0,1$ and inner solutions at $\tilde{x}_\alpha \to \pm\infty$ are overlapped and this common part have to be removed from composite solution. Therefore,

$$\{\overline{\mathbf{y}}_{\text{comp.}}\} = \{\overline{\mathbf{y}}_O\} + \{\overline{\mathbf{y}}_{\alpha=0}\} + \{\overline{\mathbf{y}}_{\alpha=1}\} - \{\overline{\mathbf{y}}_O^{\alpha=0}\} - \{\overline{\mathbf{y}}_O^{\alpha=1}\} \qquad (57)$$

where $\{\overline{\mathbf{y}}_O^{\alpha=0}\}$ and $\{\overline{\mathbf{y}}_O^{\alpha=1}\}$ are common parts of inner and outer solutions at two ends of the shell which can be determined by definition of intermediate variable or Van-Dyke's matching principle [34]. Eight constants, consist of three constants in general solution of each boundary and two constants $\overline{c}_0$ and c_7, should be calculated by the boundary conditions. The clamed boundary conditions in (i) th order perturbation solution are:

$$\overline{x} = 0 \ (\tilde{x}_0 = 0) \to \overline{u}_{0i}, \overline{\varphi}_{0i}, \overline{w}_{0i}, \overline{\psi}_{0i} = 0,$$
$$\overline{x} = 1 \ (\tilde{x}_1 = 0) \to \overline{u}_{1i}, \overline{\varphi}_{1i}, \overline{w}_{1i}, \overline{\psi}_{1i} = 0 \qquad (58)$$

Finally, the unknown vector $\{\overline{\mathbf{y}}\} = \{\overline{\mathbf{y}}_{\text{comp.}}\} = \{\overline{u}, \overline{\varphi}, \overline{w}, \overline{\psi}\}$ which consists of dimensionless displacement field components would be obtained in terms of $\overline{x}$ and $\overline{z}$ variables. Considering Eq. (4) and $\overline{U}_{z,x} = U_{z,x}/h_0$, the dimensionless

radial and axial displacements can be calculated. Using Eqs. (5-9) would yield $[\mathbf{F}], [\mathbf{C}], I_{1,2,3}, J$ and $[\mathbf{E}]$, respectively. The hydrostatic pressure, strain energy function and second Piola–Kirchhoff stress distribution could be calculated by using Eqs. (14), (16) and (17). The relation $[\boldsymbol{\sigma}] = (1/J)[\mathbf{F}][\mathbf{S}][\mathbf{F}]^{\text{T}}$ would result in Cauchy stress components. The analytical solution has been carried out by writing the program in MAPLE 18 software.

4. Numerical results and discussion

4.1. Finite Element (FE) solution

In order to demonstrate the potentials of the presented analytical solution for the purpose of analyzing pressurized thick cylinder with variable thickness made of nearly compressible hyperelastic material, a numerical solution based on Finite Element Method (FEM) is investigated. The ANSYS 16 package is used in the static analysis of thick hollow cylinder with variable thickness under non-uniform internal pressure and clamped boundary conditions. The PLANE183 element in the axisymmetric mode, which is an element with eight nodes and two translational degrees of freedom in the axial and radial directions per each node, has been used to model the mechanical part of the analysis. It also has mixed formulation capability for simulating deformations of nearly incompressible hyperelastic materials. In order to consider Mooney-Rivlin elastic model in nearly incompressible condition, three constants involving C_{10}, C_{01} and d should be defined for ANSYS software. Two first constants are the same material properties as C_1 and C_2 in Eq. (13), respectively. d is material incompressibility parameter which relation with bulk modulus is $k.d = 2$ [13]. For non-uniform internal pressure, the pressure functions have been defined and applied to the internal layer nodes. Clamped boundary conditions have been exerted by preventing the nodes around the two ends of the cylinder from movement. In the next sections, the numerical results (FEM) and analytical results (MAE) have been investigated for different case studies.

4.2. Constant thickness-Uniform pressure

As a case study, a thick homogenous cylinder with constant thickness under uniform internal pressure and clamped-clamped boundary conditions at the two ends with the following geometry characteristics have been considered: $R = 50\,\text{mm}$, $h = 6\,\text{mm}$ and $L = 400\,\text{mm}$. The constants of Mooney-Rivlin model for rubber assume

$$C_1 = 0.552\,\text{MPa}\,(80\,\text{psi}) \qquad \text{and} \qquad C_2 = 0.138\,\text{MPa}\,(20\,\text{psi})$$

[9,16,29]. The applied uniform internal pressure is $P_i = 8\,\text{kPa}$. The following changes should be applied for constant thickness and uniform pressure in the equations of inner and outer solutions (in section 3)

$$\{\mathbf{F}_{O1}^{II'}\} = \{\mathbf{F}_{\alpha 1}^{DA\alpha}\} = \{\mathbf{F}_{\alpha 1}^{DII\alpha}\} = \{\mathbf{F}_{\alpha 1}^{P\alpha}\} = \{\mathbf{F}_{\alpha 1}^{DP\alpha}\} = 0 \qquad (59)$$

$$\begin{aligned} \overline{P}_i(x) &= \overline{P}_{i\alpha} = \overline{P}_i, \\ \overline{R}(x) &= \overline{R}_\alpha = \overline{R}, \\ \overline{h}(x) &= \overline{h}_\alpha = \overline{h}, \\ \overline{II}_\alpha &= \overline{II} \end{aligned} \qquad (60)$$

Various relations are recommended for estimating the value of incompressibility parameter k. The common part of similar relations is definition of the bulk modulus based on material model constants (C_1 and C_2 in current model) or initial shear modulus (G) and Poisson's ratio (ν). In nearly incompressible materials, Poisson's ratio with respect to compressibility intensity consider about $\nu = 0.49 - 0.499$ [4,12,16]. The compressibility parameter k only scales the penalty functions (but no change in shapes) and enforces incompressibility if large values are chosen. Therefore, the order of bulk modulus can be estimated based on compressibility intensity:

$$\nu = 0.49 \rightarrow k \propto 2(C_1 + C_2) \times 10^2$$
$$\text{or} \qquad\qquad\qquad\qquad\qquad\qquad\qquad (61)$$
$$\nu = 0.499 \rightarrow k \propto 2(C_1 + C_2) \times 10^3$$

Considering C_1 and C_2 values in current research lead in the variation range of the k about $1 - 100\,\text{MPa}$. Although constants C_1, C_2 and k can be calculated independently from experimental tests [14], exact k is considered based on the convergence of solutions at nearly incompressible limit in current study [7,8].

The difference percentage of dimensionless radial displacement resulting from the numerical and analytical solution i.e. $\text{Diff}\,\bar{U}_z(\%) = \left| \left(\bar{U}_z{}^{\text{MAE}} - \bar{U}_z{}^{\text{FEM}} \right) / \bar{U}_z{}^{\text{FEM}} \right| \times 100$ with respect to k for different $\bar{R}$ and P_i/C_{12} are plotted in Fig. 2. Variation range of k is considered $5 - 100\,\text{MPa}$. Important remark is that for $k < 5\,\text{MPa}$, the eigenvalues of characteristic equation no longer have conjugate complex form and MAE solution diverge. Fig. 2(a) shows that ascending increment in the ratio of middle layer radius to thickness increase difference percentage of MAE and FEM for different k. Furthermore, the variation of bulk modulus is in a manner that for all the values of $\bar{R}$ and P_i/C_{12}, the least difference percentage is observed at a definite value of k. The value of this point is $k = 10\,\text{MPa}$ for any $\bar{R}$ and P_i/C_{12}. It is observed that the accuracy of MAE descend for $\bar{R} > 15$ because of intensifying nonlinear behaviour of the cylinder. For $\bar{R} < 3$, FSDT accuracy decrease in analyzing thick cylindrical shells. It can be seen from Fig. 2(b) that increasing the ratio of pressure to material constants (material strength) cause an increase in difference percentage between MAE and FEM solution for different k. This value is in the estimated range for nearly incompressible Mooney-Rivlin hyperelastic model with $C_1 = 0.552\,\text{MPa}$ and

$C_2 = 0.138\,\text{MPa}$ material constants and lead in convergence between MAE and FEM results. The same manner has been observed for difference percentage of dimensionless axial displacement. Therefore, we set $k = 10\,\text{MPa}$ in the current study.

4.3. Variable thickness-Uniform pressure

A thick homogenous cylinder with variable thickness under uniform internal pressure and clamped-clamped boundary conditions with the geometry of: $r_i = 47\,\text{mm}$, $h_a = 12\,\text{mm}$, $h_b = 6\,\text{mm}$ and $L = 400\,\text{mm}$ have been investigated. The constants of nearly incompressible Mooney-Rivlin model for rubber assume $C_1 = 0.552\,\text{MPa}$, $C_2 = 0.138\,\text{MPa}$ and $k = 10\,\text{MPa}$. The applied uniform internal pressure is $P_i = 8\,\text{kPa}$ as previous section. The following changes should be applied for uniform pressure in the inner and outer equations (in section 3)

$$\left\{ \mathbf{F}_{\alpha 1}^{\text{D}P\alpha} \right\} = 0, \quad \bar{P}_i(x) = \bar{P}_{i\alpha} = \bar{P}_i \qquad (62)$$

Dimensionless Cauchy stresses and hydrostatic pressure are defined as $\bar{\boldsymbol{\sigma}} = \boldsymbol{\sigma}/P_i$, $\bar{P} = P/P_i$.

Dimensionless radial displacement distribution along axial direction and thickness of shell in different layers are plotted in Fig. 3. Radial displacements decrease from internal layer to the external one in any thickness. Variation of the displacements increases in thinner parts of shell. At the points far away from boundaries, this variation is uniform because of linear thickness variation. However, non-uniform peak is observed around boundaries under the effect of shear stresses and clamped B.C. As explain in Fig. 2, difference of MAE and FEM results increase at higher thickness ($\bar{R}$) toward low values of $\bar{x}$.

Fig. 4 shows the dimensionless axial displacement distribution along axial direction and thickness of shell in different layers. Axial displacement is zero at the middle of cylinder and increase uniformly toward the boundaries at the points far away from boundaries. Although displacements are zero at $\bar{x} = 0,1$, shear stresses near boundaries intensify axial displacements. Fig. 4(a) reveals that axial displacements at the points far away from boundaries are equal for different layers, however displacements differ at layers around boundaries and maximum value occur at inner layer (close to loading). Axial displacements show uniform distribution along thickness toward $\bar{x} = 0.5$ while toward the boundaries reverse bolds true. One half of the cylinder is always in tension and other in compression. As $\bar{x}$ increase, by descending thickness, FSDT accuracy decrease.
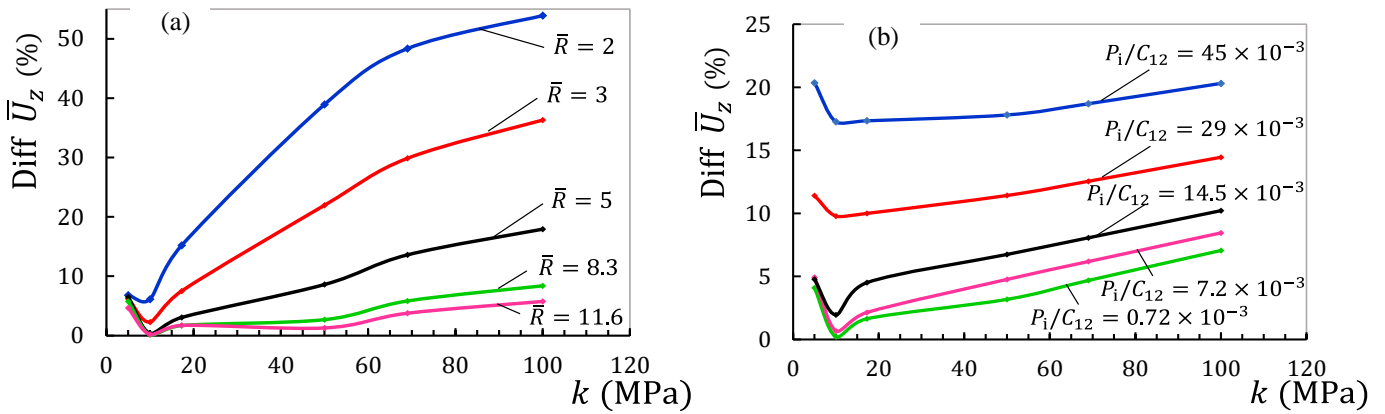
Figure 2. Difference percentage of radial displacement with respect to k for different (a) $\bar{R}$ and (b) P_i/C_{12}
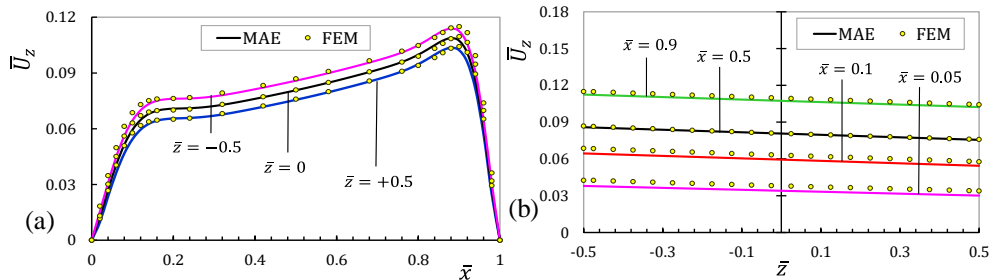
Figure 3. Dimensionless radial displacement distribution (a) along axial direction (b) along thickness
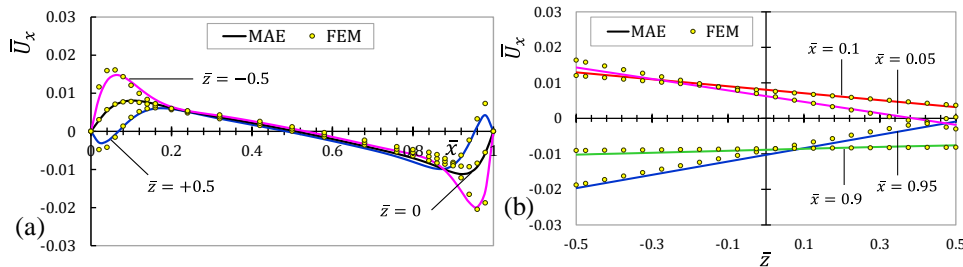
Figure 4. Dimensionless axial displacement distribution (a) along axial direction (b) along thickness

Fig. 5(a) and (b) show dimensionless circumferential and axial Cauchy stress distribution in different layers along axial direction of cylinder, respectively. Nearly all parts of the shell have tensile circumferential and axial Cauchy stress, except around boundaries at the outer layer. It can be estimated that similar manner occur at the inner layer points for external pressure load. Because all the elements are in tensile state, but clamped conditions near boundaries at the layer away from loading cause resistance against displacement which lead in compressive stresses. It is obviously observed that the maximum stress values are axial stress around boundary $\bar{x} = 1$ which has minimum thickness. The circumferential stress of the points away from boundaries have higher variation than axial stress because of higher radial displacement quantities to axial ones and being away from clamped effect.

Dimensionless shear Cauchy stress distribution in different layers along axial direction is plotted in Fig. 5(c). Existence of shear stress near boundaries reveal the advantage of shear deformation theory respect to theories that neglect shear stress effect. Although FSDT is suitable for displacement analyzing rather than stress one, the results of MAE are more accurate around boundaries respect to FE solution. Inner layer of the shell is critical layer under internal pressure load. Getting away from middle layer, especially toward critical layer, change linear distribution of displacements and stresses to nonlinear state. By the way, stresses are calculated indirectly from displacements and strains in shear deformation theory. Therefore, first-order shear deformation theory estimate stresses more slightly than real states in critical layers. The distribution of the dimensionless hydrostatic pressure in different layers along axial direction is plotted in Fig. 5(d). Hydrostatic pressure can be considered as average of principal stresses. Investigation and comparison of Fig. 5 confirm this fact; so hydrostatic pressure can be a suitable equivalent parameter that show shell state from the view point of stresses. Therefore, similar to axial and circumferential stresses, nearly all parts of the shell have positive values of hydrostatic pressure except around boundaries at the outer layer away from loading. Difference between MAE and FEM results increase at the points of internal and external layers away from boundaries. Increasing $\bar{x}$ (descending thickness) leads in continuous increment of hydrostatic pressure way from boundaries because of higher displacement values at smaller thickness. Considering Eq. (14) and hydrostatic pressure distribution lead in $0.995 < J < 1.007$.
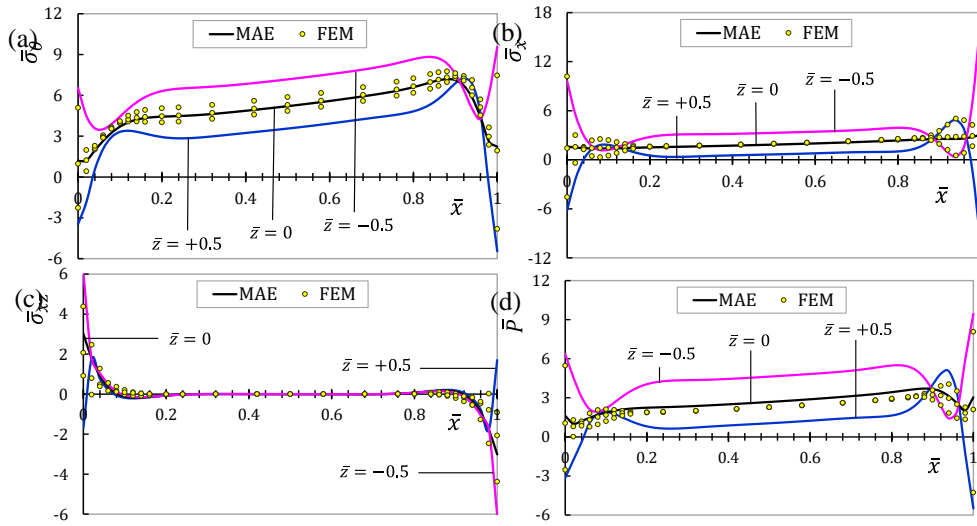
Figure 5. Dimensionless (a) circumferential Cauchy stress, (b) axial Cauchy stress, (c) shear Cauchy stress and (d) hydrostatic pressure in different layers along axial direction

4.4. Variable thickness-Non-uniform pressure

In order to report the performance of current study for analyzing arteries, we consider the mechanical response of a hyperelastic thick-walled circular cylindrical tube under various pressure loads with clamped end conditions to periphery tissues. As current research studies the manner of pressurized vessels in dimensionless state, the results of FSDT and MAE solution may be suitable for investigating some proper case studies of blood vessels. Considering the applicability of the rubber elasticity theory to aortic soft tissues such as elastin, the behaviour of blood vessels under non-uniform pressure distribution has been investigated from current research. Furthermore, the current study will present helpful results for alternative hyperelastic materials with higher strength for blood vessels in future research [22,24,35].

In general, arteries are roughly subdivided into two types: elastic and muscular. Elastic arteries have relatively large diameters and are located close to the heart (for example, the aorta and the carotid and iliac arteries), while muscular arteries are located at the periphery. Depending on the type of artery considered, the material behaviour may be regarded as (perfectly) elastic for proximal arteries of the elastic type, or viscoelastic for distal arteries of the muscular type. Here we focus attention on the elastic arterial walls composed of three distinct layers, the intima (inner) layer, the media (middle) layer and the adventitia (outer) layer. From the mechanical perspective, the media is the most significant layer in a healthy artery. The thickness of the layers depends strongly on the type (elastic or muscular) and the physiological function of the blood vessel and its topographical site. Although the mechanical properties of arterial walls vary along the arterial layers, the general mechanical characteristics exhibited by arterial walls are the same. Hence, Most of the constitutive models treat the arterial wall as a single layer. Since arteries have no valuable changes in volume within the physiological range of deformation, they can be regarded as nearly incompressible materials [36].

It is known that pathological changes of the intimal components may be associated with atherosclerosis, the most common disease of arterial walls, which involves deposition of fatty substances, calcium, collagen fibers, cellular waste products and fibrin (a clotting material in the blood). The resulting build-up is called atherosclerotic plaque. It may be very complex in geometry and biochemical composition. The mechanical behaviour of atherosclerotic arteries differs significantly from that of healthy arteries. In later stages the media is also affected. These pathological changes are associated with significant alterations in the mechanical and geometrical properties of the arterial wall. The layers thicken and stiffen with age (arteriosclerosis) so that the variation of thickness and physiological pressure occur in blood vessels [36,37]. In this study, the mechanical effects of pathological changes of the thickened and stiffened layers due to arteriosclerosis containing atherosclerotic plaque were considered. Hence, it would be interesting to apply the displacement and stress analysis performed in this study to the prediction of diameter growth and rupture in atherosclerotic arteries. Furthermore, dilation of an artery using a balloon catheter during mechanical treatments such as percutaneous transluminal angioplasty with loading in the physiological range of deformation can be estimated by current method [26,27]. Wall shearing may take place in balloon angioplasty and the relative sensitivity of wall displacement and stress to geometrical and loading properties of the aneurysmal tissue in clinical interventions can be evaluated [36].

According to the explanation presented, a thick homogenous cylinder with variable thickness and clamped boundary conditions by the similar geometry and material constants as previous section is considered. Internal pressure distribution, unlike previous case studies, varies non-uniformly along axial direction of vessel. Five pressure profiles are applied to the cylindrical shell. Table 1 shows the characteristic of applied pressures. The pressure profiles vary in the range of $5\,\mathrm{kPa}(40\,\mathrm{mmHg}) - 13\,\mathrm{kPa}(100\,\mathrm{mmHg})$ which are the mean blood vessel pressures of human soft tissues. $100\,\mathrm{mmHg}$ is the mean of systolic/diastolic pressure [35,38] and $40\,\mathrm{mmHg}$ may be occurred in hypotension pressure of arteries [39,40]. There are many isotropic rubber-like potentials proposed for carotid arteries (such as current study) which are able to model the behaviour of blood vessels in the physiological pressure domain [36,41]. Although the material models of arteries have commonly exponential form, simple neo-Hookean model with material constant $G/2$ (similar to current model) in some research is considered for isotropic parts of blood vessels. Material properties, applied pressures and geometry of various

arteries may be in $4 < \bar{R} < 10$ and $0.02 < P_i/G < 20$ range [26,27,36,37]. Hence, case studies of variable thickness are selected similar to geometry of common elastic arteries $\bar{R}$ (as

unite layer) in current research; means that the thick and thin part of the vessel cover the average thickness of the layers in common elastic arteries of human body

Table 1. The characteristic of non-uniform internal pressure profiles

Pressure Profile ID	Pressure Profile Relation	Pressure constants
P_{i1}	$P_i(\bar{x}) = P_i = \text{constant}$	$P_i = 9 \text{ kPa}$
P_{i2}	$P_i(\bar{x}) = P_i^0 - \left(P_i^0 - P_i^1\right)\bar{x}$	$P_i^0 = 13 \text{ kPa},\ P_i^1 = 5 \text{ kPa}$
P_{i3}	$P_i(\bar{x}) = P_i^0 - \left(P_i^0 - P_i^1\right)\bar{x}^2$	$P_i^0 = 13 \text{ kPa},\ P_i^1 = 5 \text{ kPa}$
P_{i4}	$P_i(\bar{x}) = P_i^{01} - 4\left(P_i^{01} - P_i^{0.5}\right)\left(\bar{x} - \bar{x}^2\right)$	$P_i^{01} = 5 \text{ kPa},\ P_i^{0.5} = 13 \text{ kPa}$
P_{i5}	$P_i(\bar{x}) = P_i^{01} - \left(P_i^{01} - P_i^{0.5}\right)\sin\left(\pi\bar{x}\right)$	$P_i^{01} = 13 \text{ kPa},\ P_i^{0.5} = 5 \text{ kPa}$

Distribution of non-uniform internal pressures along axial direction are depicted in Fig. 6. The pressure profiles are considered coordinated by the linear thickness variation of shell. Fig. 7 show dimensionless radial and axial displacement distribution in middle layer along axial direction for different pressure profiles. Dimensionless hydrostatic pressure values for different pressures distribution are presented in Tables 2. In the constant pressure $P_{i1} = 9$ kPa (mean value of 5 and 13 kPa), as previous results, thinner parts of vessel cause more radial displacement. Linear variation of pressure P_{i2} and thickness $h(\bar{x})$ of shell are in reverse directions and counteract each other effect. Therefore, P_{i2} cause uniform distribution of radial displacement along axial direction of shell with linear variable thickness. This counterbalance is to some extent that despite the existence of 13 kPa pressure at $\bar{x} = 0$, with respect to $P_{i1} = 9$ kPa, maximum value of displacement descend. Considering Figs. 6 and 7 show that parabolic pressure P_{i3} compared with linear one P_{i2} has higher values of pressure and consequently displacement all over the length of shell. Radial displacement under P_{i2} and P_{i3} decrease toward right boundary linearly and nonlinearly (similar to parabolic variation) respectively. It can be observed that maximum displacement resulting from P_{i1} are higher than P_{i2} and P_{i3}. Pressure profiles of P_{i4} and P_{i5} which have higher non-uniform distribution than other pressures lead in larger displacement values respect to constant pressure P_{i1}. By similar range of applied variable pressure, more non-uniform pressure distribution along the longitudinal direction cause higher amount of radial displacements. In this state, displacement values along the length of shell have more difference. Therefore, important conclusion is that similar profile of variable thickness and non-uniform applied pressure result in minor displacement quantities and uniform displacement distributions. In the current case studies, strength of the cylinder with linear variable thickness from the view point of less radial displacements across non-uniform pressure has following arrangement:

$$P_{i5} < P_{i4} < P_{i1} < P_{i3} < P_{i2} \tag{63}$$

Whatever pressure distribution be symmetric in axial direction, the positive and negative axial displacements have more equal contribution along the length of shell. The contribution of tensile elements in axial direction are more than compressive ones under asymmetric pressures P_{i2} and P_{i3}. The

elements have nearly equal stretch along axial direction at points away from boundaries, especially for more uniform pressure distributions. Strength of the cylinder with linear variable thickness from the view point of uniform and low axial displacement distribution across non-uniform pressure has following arrangement:

$$P_{i3} < P_{i2} < P_{i4} < P_{i5} < P_{i1} \tag{64}$$

The points of internal layer with minimum thickness and maximum displacement are critical elements in nearly incompressible hyperelastic cylinder with variable thickness under non-uniform internal pressure. Furthermore, similar distribution of pressure and thickness could be a suitable criterion in designing thickness profile of pressurized vessels. Hydrostatic pressure of internal layer has its maximum value at $\bar{x} = 0$ for P_{i2} and P_{i3} unexpectedly, because the effect of pressure profile is dominant to variable thickness. For other profiles, maximum hydrostatic pressure occurs at $\bar{x} = 1$ because of lower thickness. P_{i4} and P_{i5} cause minimum and maximum hydrostatic pressure among the profiles in current study, respectively. Therefore, vessels with variable thickness have minor hydrostatic pressure under non-uniform pressure distribution with peak away from boundaries.

This approach enables insight into the nature of the deformation and stress distribution across the arterial wall to be gained, and therefore offers the potential for study of the mechanical functionality of arteries in physiological pressure range. The obtained analysis represents useful results for the community of vascular biomechanics. In particular, we use an analysis to examine the inflation of a cylindrical tube at various internal pressure profiles and to compute the evolution of the inner radius (critical layer) with the internal pressure. In addition, at the approximate physiological pressures, we evaluate the effect of variable thickness on the tube and determine the effect of the shear stress at the surfaces. It can be mentioned that our results tend to emphasize on wall degeneration of arteries within the aneurysm wall [36,37] that affects the thickness profile of the tissue, which can be mostly analyzed as variable thickness blood vessels. The rupture modes in the aortic specimens are characterized by oblique tears in the circumferential direction, indicating that the failure of the aneurismal aortic tissue is mainly governed by the axial stress. The failure stress in the axial direction is much higher in the adventitia layer compared to that in the media layer [37]. This means that the failure in the aneurismal aortic tissue may initiate in the media layer; i.e. inner surface of arteries are critical one which proved by current results (section 4.3 and

4.4). It is considered that the current methodology could have potential to identify the aneurismal wall displacement and stress and to assess the aortic aneurysm rupture risk based on maximal diameter, axial stress and hydrostatic pressure (as mean stress) in both constant and variable thickness vessels for patients having an aneurysm.
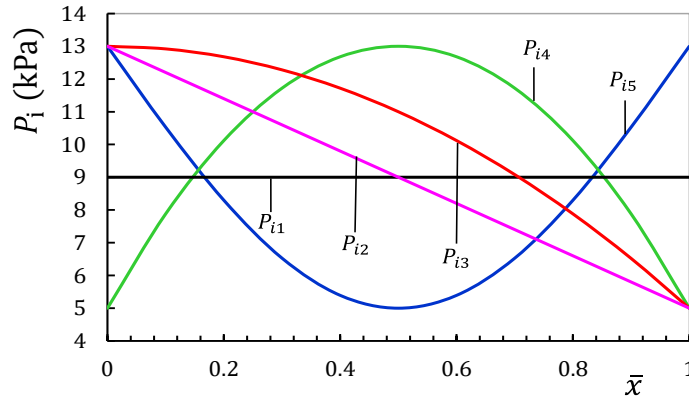
Figure 6. Distribution of different non-uniform internal pressures along axial direction
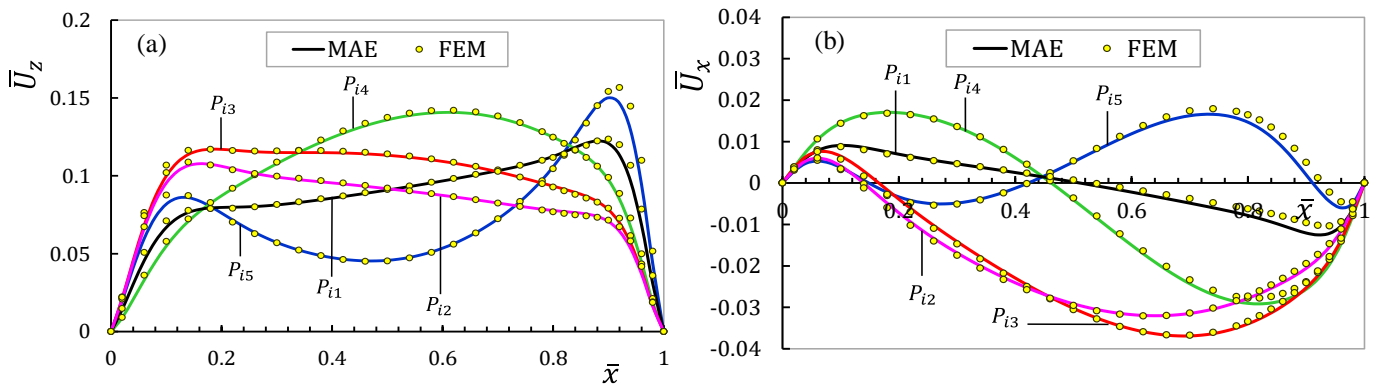
Figure 7. Dimensionless (a) radial displacement (b) axial displacement in middle layer along axial direction for various load

Table 2. Dimensionless hydrostatic pressure for different internal pressure profiles

P / P_{i1}	$\bar{z} = -0.5$				$\bar{z} = 0$			
	$\bar{x} = 0$	$\bar{x} = 0.3$	$\bar{x} = 0.7$	$\bar{x} = 1$	$\bar{x} = 0$	$\bar{x} = 0.3$	$\bar{x} = 0.7$	$\bar{x} = 1$
P_{i1}	5.601	2.908	3.629	8.367	1.282	2.088	2.865	2.467
P_{i2}	8.105	3.530	2.814	5.865	1.297	2.349	2.426	2.287
P_{i3}	8.373	4.275	3.685	6.526	1.526	2.761	2.979	2.751
P_{i4}	4.526	3.982	4.861	6.604	1.479	2.719	3.696	3.015
P_{i5}	7.524	1.962	2.552	11.178	1.123	1.534	2.132	1.926

5. Conclusions

In current research, the homogeneous and isotropic hyperelastic hollow cylinders with variable thickness under nearly incompressible condition have been analyzed by FSDT. Two ends of thick-walled vessel have clamped boundary conditions and non-uniform internal pressure load is applied along internal layer. Two-term Mooney-Rivlin type material is considered which is a suitable hyperelastic model for rubbers. In the present case, the extension of incompressible materials to nearly incompressible materials is considered; means that the incompressibility constraint is replaced with a penalty function correspond to the constraint $J = 1$ in strain energy density function. In this context, it can be interpreted as a penalty parameter that enforces incompressibility if large values are chosen respect to hyperelastic material constants. Match Asymptotic Expansion (MAE) of the perturbation theory is used for solving the governing equations. The advantages of this method are fast convergence, closed form solution and compatibility with physics of shell. It can explain the behaviour of the shell successfully even near the boundaries. MAE in perturbation theory converts a system of four nonlinear coupled differential equations with variable coefficients to boundary layer in two region of solution near boundaries and a solution away from boundaries. A new ingenious formulation and parameters have been defined during current study to simplify and abbreviate the representation of inner and outer equations components in MAE. In addition, the terms of variable thickness and non-uniform pressure have been presented in special representation. Displacement, stress and hydrostatic pressure distributions resulting from MAE solution have been presented for some case studies and the results have been compared with a FEM modeling in ANSYS software. The results prove the effectiveness of FSDT and MAE combination to derive and solve the governing equations of nonlinear problems such as nearly incompressible hyperelastic shells. The shear stress in boundary areas cannot be ignored, unlike

areas away from the boundaries. The calculus of stresses from displacements and strains by using nonlinear constitutive relations may be decreased the accuracy respect to displacements results. Validity range of current analysis is about $3 < \bar{R} < 15$ for geometry and $P_i / C_{12} < 0.03$ for loading of variable thickness pressure vessels. Actually, intensifying nonlinear state of the cylinder descend FSDT and MAE accuracy in analyzing the shell, simultaneously. The behaviour of blood vessels under non-uniform pressure distribution shows that similar profile of variable thickness and non-

uniform applied pressure result in minor displacement quantities and uniform displacement distributions which could be a suitable criterion in designing thickness profile of pressurized vessels. Furthermore, vessels with variable thickness have minor hydrostatic pressure and stresses under non-uniform pressure distribution with peak away from boundaries. Current study aims to illustrate the performance of the potentials and their reliability for the prediction of the state of deformation and stress in hyperelastic vessels from rubbers to arteries.

Appendix

The non-homogeneity vectors of $O(\varepsilon^2)$ equations in outer and inner expansions are as follows:

$$
\begin{aligned}
\left\{\mathbf{F}_{O1}^{II}\right\}_1 &= Ck_3\Big[\big(\overline{II}(2,-1)+\overline{II}(0,1)\big)\bar{\psi}_{O0}{}^2 + 2\overline{II}(1,-1)\bar{w}_{O0}\bar{\psi}_{O0} + 2\big(\overline{II}(1,0)+\overline{II}(0,1)\big)\bar{v}_{O0}\bar{\psi}_{O0} \\
&\quad + 2\overline{II}(0,0)\bar{v}_{O0}\bar{w}_{O0} + \overline{II}(0,-1)\bar{w}_{O0}{}^2\Big] + Ck_7\Big[\overline{II}(1,0)\bar{\psi}_{O0}{}^2 + \overline{II}(0,0)\bar{w}_{O0}\bar{\psi}_{O0}\Big] \\
&\quad - k\Big[\overline{II}(1,1)\bar{\varphi}_{O0}{}' + 2\overline{II}(0,1)\bar{v}_{O0}{}^2\Big] - \hat{K}_s C_{12}\overline{II}(0,1)\bar{\varphi}_{O0}{}^2, \qquad \left\{\mathbf{F}_{O1}^{II\,'}\right\}_1 = 0
\end{aligned}
\tag{A1}
$$

$$
\begin{aligned}
\left\{\mathbf{F}_{O1}^{II}\right\}_2 &= Ck_1\Big[\big(\overline{II}(2,0)+\overline{II}(1,1)\big)\bar{\psi}_{O0}{}' + \overline{II}(1,0)\bar{w}_{O0}{}' - \big(\overline{II}(1,0)\bar{\psi}_{O0}+\overline{II}(0,0)\bar{w}_{O0}\big)\bar{\varphi}_{O0} \\
&\quad + \hat{K}_s\overline{II}(0,1)\bar{v}_{O0}\bar{\varphi}_{O0}\Big] + K_s Ck_2\big(\overline{II}(1,0)\bar{\psi}_{O0}+\overline{II}(0,0)\bar{w}_{O0}\big)\bar{\varphi}_{O0} \\
&\quad + K_s C_{12}\big(\overline{II}(0,1)\bar{w}_{O0}{}' + \overline{II}(1,1)\bar{\psi}_{O0}{}'\big) - k\,\overline{II}(1,1)\bar{v}_{O0}{}' + \hat{K}_s k\,\overline{II}(0,1)\bar{\varphi}_{O0}\bar{\psi}_{O0} \\
\left\{\mathbf{F}_{O1}^{II\,'}\right\}_2 &= Ck_1\Big[\overline{II}{}'(2,0)\bar{\psi}_{O0} + \overline{II}{}'(1,0)\bar{w}_{O0} + \overline{II}{}'(1,1)\bar{\psi}_{O0}\Big] - k\,\overline{II}{}'(1,1)\bar{v}_{O0}
\end{aligned}
\tag{A2}
$$

$$
\begin{aligned}
\left\{\mathbf{F}_{O1}^{II}\right\}_3 &= -Ck_3\Big[\overline{II}(0,0)\big(\bar{v}_{O0}{}^2+\bar{\psi}_{O0}{}^2\big) + 2\big(\overline{II}(1,-1)\bar{\psi}_{O0}+\overline{II}(0,-1)\bar{w}_{O0}\big)\big(\bar{v}_{O0}+\bar{\psi}_{O0}\big)\Big] \\
&\quad - Ck_1\overline{II}(1,0)\bar{\varphi}_{O0}{}' - Ck_7\overline{II}(0,0)\bar{v}_{O0}\bar{\psi}_{O0} - K_s C_{12}\overline{II}(0,1)\bar{\varphi}_{O0}{}' + 2C_2\overline{II}(0,0)\bar{\varphi}_{O0}{}^2 \\
&\quad + 2k\Big[\overline{II}(2,-2)\bar{\psi}_{O0}{}^2 + 2\overline{II}(1,-2)\bar{w}_{O0}\bar{\psi}_{O0} + \overline{II}(0,-2)\bar{w}_{O0}{}^2\Big] \\
\left\{\mathbf{F}_{O1}^{II\,'}\right\}_3 &= -K_s C_{12}\overline{II}{}'(0,1)\bar{\varphi}_{O0}
\end{aligned}
\tag{A3}
$$

$$
\begin{aligned}
\left\{\mathbf{F}_{O1}^{II}\right\}_4 &= -Ck_1\big(\overline{II}(2,0)+\overline{II}(1,1)\big)\bar{\varphi}_{O0}{}' - K_s C_{12}\overline{II}(1,1)\bar{\varphi}_{O0}{}' - Ck_3\Big[\overline{II}(2,-1)\,\bar{\psi}_{O0}\big(3\bar{\psi}_{O0}+2\bar{v}_{O0}\big) \\
&\quad + \overline{II}(1,0)\big(3\bar{\psi}_{O0}{}^2+\bar{v}_{O0}{}^2\big) + \overline{II}(0,1)\bar{v}_{O0}\big(2\bar{\psi}_{O0}+\bar{v}_{O0}\big) + \overline{II}(1,-1)\bar{w}_{O0}\big(4\bar{\psi}_{O0}+2\bar{v}_{O0}\big) \\
&\quad + 2\overline{II}(0,0)\bar{w}_{O0}\bar{\psi}_{O0} + 2\overline{II}(0,-1)\bar{w}_{O0}{}^2\Big] - Ck_7\Big[\overline{II}(0,0)\bar{v}_{O0}\bar{w}_{O0} + 2\overline{II}(1,0)\bar{v}_{O0}\bar{\psi}_{O0}\Big] \\
&\quad - 2C_2\overline{II}(1,0)\bar{\varphi}_{O0}{}^2 + 2k\Big[\overline{II}(1,-2)\bar{w}_{O0}{}^2 + \big(\overline{II}(3,-2)+\overline{II}(0,1)\big)\bar{\psi}_{O0}{}^2 + 2\overline{II}(2,-2)\bar{w}_{O0}\bar{\psi}_{O0}\Big] \\
\left\{\mathbf{F}_{O1}^{II\,'}\right\}_4 &= -K_s C_{12}\overline{II}{}'(1,1)\bar{\varphi}_{O0}
\end{aligned}
\tag{A4}
$$

$$
\left\{\mathbf{F}_{\alpha1}^{P\alpha}\right\}_1 = \left\{\mathbf{F}_{\alpha1}^{P\alpha}\right\}_2 = 0, \quad \left\{\mathbf{F}_{\alpha1}^{P\alpha}\right\}_3 = -\bar{P}_{i\alpha}\tilde{x}_\alpha\left(D\bar{R}_\alpha - \frac{D\bar{h}_\alpha}{2}\right), \quad \left\{\mathbf{F}_{\alpha1}^{P\alpha}\right\}_4 = \bar{P}_{i\alpha}\tilde{x}_\alpha\big(D\bar{h}_\alpha\bar{R}_\alpha + \bar{h}_\alpha D\bar{R}_\alpha - \bar{h}_\alpha D\bar{h}_\alpha\big)
\tag{A5}
$$

$$
\left\{\mathbf{F}_{\alpha1}^{DP\alpha}\right\}_1 = \left\{\mathbf{F}_{\alpha1}^{DP\alpha}\right\}_2 = 0, \quad \left\{\mathbf{F}_{\alpha1}^{DP\alpha}\right\}_3 = -D\bar{P}_{i\alpha}\tilde{x}_\alpha\left(\bar{R}_\alpha - \frac{\bar{h}_\alpha}{2}\right), \quad \left\{\mathbf{F}_{\alpha1}^{DP\alpha}\right\}_4 = \frac{D\bar{P}_{i\alpha}\tilde{x}_\alpha\bar{h}_\alpha}{2}\left(\bar{R}_\alpha - \frac{\bar{h}_\alpha}{2}\right)
\tag{A6}
$$

$$\left\{\mathbf{F}_{\alpha 1}^{DA\alpha}\right\}_1 = \tilde{x}_\alpha C k_1 \Big[\big(D\overline{\mathit{\Pi}}_\alpha(1,0) + D\overline{\mathit{\Pi}}_\alpha(0,1)\big)\overline{\psi}_{\alpha 0} + D\overline{\mathit{\Pi}}_\alpha(0,0)\overline{w}_{\alpha 0}\Big]$$
$$-\tilde{x}_\alpha k \left(D\overline{\mathit{\Pi}}_\alpha(1,1)\overline{\varphi}_{\alpha 0}{}' + D\overline{\mathit{\Pi}}_\alpha(0,1)\overline{v}_{\alpha 0}\right) \tag{A7}$$

$$\left\{\mathbf{F}_{\alpha 1}^{DA\alpha}\right\}_2 = \tilde{x}_\alpha C k_1 \Big[\big(D\overline{\mathit{\Pi}}_\alpha(2,0) + D\overline{\mathit{\Pi}}_\alpha(1,1)\big)\overline{\psi}_{\alpha 0}{}' + D\overline{\mathit{\Pi}}_\alpha(1,0)\overline{w}_{\alpha 0}{}'\Big] + \tilde{x}_\alpha K_s C_{12}\Big[D\overline{\mathit{\Pi}}_\alpha(1,1)\overline{\psi}_{\alpha 0}{}'$$
$$+D\overline{\mathit{\Pi}}_\alpha(0,1)\big(\overline{\varphi}_{\alpha 0} + \overline{w}_{\alpha 0}{}'\big)\Big] - \tilde{x}_\alpha k \left(D\overline{\mathit{\Pi}}_\alpha(1,1)\overline{v}_{\alpha 0}{}' + D\overline{\mathit{\Pi}}_\alpha(2,1)\overline{\varphi}_{\alpha 0}{}''\right) \tag{A8}$$

$$\left\{\mathbf{F}_{\alpha 1}^{DA\alpha}\right\}_3 = -\tilde{x}_\alpha C k_1 \Big[D\overline{\mathit{\Pi}}_\alpha(1,0)\overline{\varphi}_{\alpha 0}{}' + D\overline{\mathit{\Pi}}_\alpha(0,0)\big(\overline{\psi}_{\alpha 0} + \overline{v}_{\alpha 0}\big)\Big] - \tilde{x}_\alpha K_s C_{12}\Big[D\overline{\mathit{\Pi}}_\alpha(1,1)\overline{\psi}_{\alpha 0}{}''$$
$$+D\overline{\mathit{\Pi}}_\alpha(0,1)\big(\overline{\varphi}_{\alpha 0}{}' + \overline{w}_{\alpha 0}{}''\big)\Big] + \tilde{x}_\alpha k \Big[D\overline{\mathit{\Pi}}_\alpha(0,-1)\overline{w}_{\alpha 0} + D\overline{\mathit{\Pi}}_\alpha(1,-1)\overline{\psi}_{\alpha 0}\Big] \tag{A9}$$

$$\left\{\mathbf{F}_{\alpha 1}^{DA\alpha}\right\}_4 = -\tilde{x}_\alpha C k_1 \Big[D\overline{\mathit{\Pi}}_\alpha(0,1)\big(\overline{v}_{\alpha 0}\big) + D\overline{\mathit{\Pi}}_\alpha(1,0)\big(2\overline{\psi}_{\alpha 0} + \overline{v}_{\alpha 0}\big) + D\overline{\mathit{\Pi}}_\alpha(0,0)\big(\overline{w}_{\alpha 0}\big)$$
$$+\big(D\overline{\mathit{\Pi}}_\alpha(2,0) + D\overline{\mathit{\Pi}}_\alpha(1,1)\big)\overline{\varphi}_{\alpha 0}{}'\Big] - \tilde{x}_\alpha K_s C_{12}\Big[D\overline{\mathit{\Pi}}_\alpha(2,1)\overline{\psi}_{\alpha 0}{}'' + D\overline{\mathit{\Pi}}_\alpha(1,1)\big(\overline{\varphi}_{\alpha 0}{}' + \overline{w}_{\alpha 0}{}''\big)\Big]$$
$$+\tilde{x}_\alpha k \Big[\big(D\overline{\mathit{\Pi}}_\alpha(2,-1) + D\overline{\mathit{\Pi}}_\alpha(0,1)\big)\overline{\psi}_{\alpha 0} + D\overline{\mathit{\Pi}}_\alpha(1,-1)\overline{w}_{\alpha 0}\Big] \tag{A10}$$

$$\begin{cases}\left\{\mathbf{F}_{\alpha 1}^{D\mathit{\Pi}\alpha}\right\}_2 = C k_1 \Big[\big(D\overline{\mathit{\Pi}}_\alpha(2,0) + D\overline{\mathit{\Pi}}_\alpha(1,1)\big)\overline{\psi}_{\alpha 0} + D\overline{\mathit{\Pi}}_\alpha(1,0)\overline{w}_{\alpha 0}\Big] - k \left(D\overline{\mathit{\Pi}}_\alpha(1,1)\overline{v}_{\alpha 0} + D\overline{\mathit{\Pi}}_\alpha(2,1)\overline{\varphi}_{\alpha 0}{}'\right) \\[2mm] \left\{\mathbf{F}_{\alpha 1}^{D\mathit{\Pi}\alpha}\right\}_3 = -K_s C_{12}\Big[D\overline{\mathit{\Pi}}_\alpha(1,1)\overline{\psi}_{\alpha 0}{}' + D\overline{\mathit{\Pi}}_\alpha(0,1)\big(\overline{\varphi}_{\alpha 0} + \overline{w}_{\alpha 0}{}'\big)\Big] \\[2mm] \left\{\mathbf{F}_{\alpha 1}^{D\mathit{\Pi}\alpha}\right\}_4 = -K_s C_{12}\Big[D\overline{\mathit{\Pi}}_\alpha(2,1)\overline{\psi}_{\alpha 0}{}' + D\overline{\mathit{\Pi}}_\alpha(1,1)\big(\overline{\varphi}_{\alpha 0} + \overline{w}_{\alpha 0}{}'\big)\Big], \quad \left\{\mathbf{F}_{\alpha 1}^{D\mathit{\Pi}\alpha}\right\}_1 = 0\end{cases} \tag{A11}$$

$$\left\{\mathbf{F}_{\alpha 1}^{\mathit{\Pi}\alpha}\right\}_1 = C k_3 \Big[2\big(\big(\overline{\mathit{\Pi}}_\alpha(1,1) + \overline{\mathit{\Pi}}_\alpha(2,0)\big)\overline{\psi}_{\alpha 0} + \overline{\mathit{\Pi}}_\alpha(1,0)\overline{w}_{\alpha 0}\big)\overline{\varphi}_{\alpha 0}{}' + \big(\overline{\mathit{\Pi}}_\alpha(0,1) + \overline{\mathit{\Pi}}_\alpha(2,-1)\big)\overline{\psi}_{\alpha 0}{}^2$$
$$+2\big(\overline{\mathit{\Pi}}_\alpha(1,0) + \overline{\mathit{\Pi}}_\alpha(0,1)\big)\overline{v}_{\alpha 0}\overline{\psi}_{\alpha 0} + 2\overline{\mathit{\Pi}}_\alpha(1,-1)\overline{w}_{\alpha 0}\overline{\psi}_{\alpha 0} + 2\overline{\mathit{\Pi}}_\alpha(0,0)\overline{v}_{\alpha 0}\overline{w}_{\alpha 0} + \overline{\mathit{\Pi}}_\alpha(0,-1)\overline{w}_{\alpha 0}{}^2\Big]$$
$$-C_{12}\Big[K_s\overline{\mathit{\Pi}}_\alpha(1,1)\overline{\varphi}_{\alpha 0}\overline{\psi}_{\alpha 0}{}' + \overline{\mathit{\Pi}}_\alpha(0,1)\big(K_s\overline{\varphi}_{\alpha 0}\overline{w}_{\alpha 0}{}' + \hat{K}_s\overline{\varphi}_{\alpha 0}{}^2\big)\Big]$$
$$-k\Big[2\overline{\mathit{\Pi}}_\alpha(2,1)\big(\overline{\varphi}_{\alpha 0}{}'\big)^2 + 4\overline{\mathit{\Pi}}_\alpha(1,1)\big(4\overline{v}_{\alpha 0}\overline{\varphi}_{\alpha 0}{}' - \overline{\varphi}_{\alpha 0}\overline{\psi}_{\alpha 0}{}'\big) + \overline{\mathit{\Pi}}_\alpha(0,1)\big(2\overline{v}_{\alpha 0}{}^2 - \overline{\varphi}_{\alpha 0}\overline{w}_{\alpha 0}{}'\big)\Big]$$
$$+C k_7 \Big[\overline{\mathit{\Pi}}_\alpha(1,0)\overline{\psi}_{\alpha 0}{}^2 + \overline{\mathit{\Pi}}_\alpha(0,0)\overline{w}_{\alpha 0}\overline{\psi}_{\alpha 0}\Big] \tag{A12}$$

$$\left\{\mathbf{F}_{\alpha 1}^{\mathit{\Pi}\alpha}\right\}_2 = C k_1 \big(\overline{\mathit{\Pi}}_\alpha(1,0)\overline{\psi}_{\alpha 0} + \overline{\mathit{\Pi}}_\alpha(0,0)\overline{w}_{\alpha 0} + \hat{K}_s\overline{\mathit{\Pi}}_\alpha(0,1)\overline{v}_{\alpha 0}\big)\overline{\varphi}_{\alpha 0} + K_s C k_2 \Big[\overline{\mathit{\Pi}}_\alpha(2,0)\overline{\psi}_{\alpha 0}\overline{\psi}_{\alpha 0}{}'$$
$$+\overline{\mathit{\Pi}}_\alpha(1,0)\big(\big(\overline{w}_{\alpha 0}\overline{\psi}_{\alpha 0}\big)' + \overline{\psi}_{\alpha 0}\overline{\varphi}_{\alpha 0}\big) + \overline{\mathit{\Pi}}_\alpha(0,0)\big(\overline{\varphi}_{\alpha 0} + \overline{w}_{\alpha 0}{}'\big)\overline{w}_{\alpha 0}\Big] + C k_5\overline{\mathit{\Pi}}_\alpha(2,1)\overline{\psi}_{\alpha 0}{}'\overline{\varphi}_{\alpha 0}{}'$$
$$+K_s C k_4 \Big[\overline{\mathit{\Pi}}_\alpha(0,1)\big(\overline{\psi}_{\alpha 0} + \overline{v}_{\alpha 0}\big)\overline{w}_{\alpha 0}{}' + \overline{\mathit{\Pi}}_\alpha(1,1)\big(\overline{v}_{\alpha 0} + \overline{\psi}_{\alpha 0}\big)\overline{\psi}_{\alpha 0}{}'\Big]$$
$$-K_s C_{12}\big(\overline{\mathit{\Pi}}_\alpha(2,1)\overline{\psi}_{\alpha 0}{}'' + \overline{\mathit{\Pi}}_\alpha(1,1)\overline{w}_{\alpha 0}{}''\big)\overline{\varphi}_{\alpha 0} + C k_6 \Big[\overline{\mathit{\Pi}}_\alpha(3,0)\big(\overline{\psi}_{\alpha 0}\overline{\varphi}_{\alpha 0}{}'\big)' + \overline{\mathit{\Pi}}_\alpha(2,1)\overline{\psi}_{\alpha 0}\overline{\varphi}_{\alpha 0}{}''$$
$$+\overline{\mathit{\Pi}}_\alpha(1,1)\big(\big(\overline{\psi}_{\alpha 0}\overline{v}_{\alpha 0}\big)' + \overline{\psi}_{\alpha 0}\overline{\varphi}_{\alpha 0}{}'\big) + \overline{\mathit{\Pi}}_\alpha(1,-1)\overline{w}_{\alpha 0}\overline{v}_{\alpha 0}{}' + \overline{\mathit{\Pi}}_\alpha(2,-1)\big(\overline{w}_{\alpha 0}\overline{\psi}_{\alpha 0}\big)'$$
$$+\overline{\mathit{\Pi}}_\alpha(1,0)\big(\overline{w}_{\alpha 0}\overline{v}_{\alpha 0}\big)' + \overline{\mathit{\Pi}}_\alpha(3,1)\overline{\psi}_{\alpha 0}\overline{\psi}_{\alpha 0}{}' + \overline{\mathit{\Pi}}_\alpha(2,0)\big(\big(\overline{v}_{\alpha 0}\overline{\psi}_{\alpha 0}\big)' + \big(\overline{w}_{\alpha 0}\overline{\varphi}_{\alpha 0}{}'\big)'\big)\Big]$$
$$-k\Big[\hat{K}_s\overline{\mathit{\Pi}}_\alpha(0,1)\overline{\varphi}_{\alpha 0}\overline{\psi}_{\alpha 0} + \overline{\mathit{\Pi}}_\alpha(2,1)\big(4\big(\overline{v}_{\alpha 0}\overline{\varphi}_{\alpha 0}{}'\big)' + K_s\overline{\psi}_{\alpha 0}{}'\overline{\varphi}_{\alpha 0}{}' - \overline{\varphi}_{\alpha 0}\overline{\psi}_{\alpha 0}{}''\big)$$
$$+\overline{\mathit{\Pi}}_\alpha(1,1)\big(4\overline{v}_{\alpha 0}\overline{v}_{\alpha 0}{}' - \overline{\varphi}_{\alpha 0}\overline{w}_{\alpha 0}{}'' + \hat{K}_s\big(\overline{w}_{\alpha 0}{}' + \overline{\varphi}_{\alpha 0}\big)\overline{\varphi}_{\alpha 0}{}'\big) + 4\overline{\mathit{\Pi}}_\alpha(3,1)\overline{\varphi}_{\alpha 0}{}'\overline{\varphi}_{\alpha 0}{}''\Big]$$
$$+C k_7 \Big[2\overline{\mathit{\Pi}}_\alpha(2,0)\overline{\psi}_{\alpha 0}\overline{\psi}_{\alpha 0}{}' + \overline{\mathit{\Pi}}_\alpha(1,0)\big(\overline{w}_{\alpha 0}\overline{\psi}_{\alpha 0}\big)'\Big] \tag{A13}$$

$$
\begin{aligned}
\left\{\mathbf{F}_{\alpha 1}^{II_\alpha}\right\}_3 = C k_1 \Bigg[&\overline{II}_\alpha(2,0)\bar{\psi}_{\alpha 0}\bar{\psi}_{\alpha 0}'' + \overline{II}_\alpha(1,0)\left(\bar{w}_{\alpha 0}'\bar{\psi}_{\alpha 0}' + \bar{w}_{\alpha 0}\bar{\psi}_{\alpha 0}'' + \bar{\psi}_{\alpha 0}\bar{w}_{\alpha 0}''\right) + 2\overline{II}_\alpha(0,0)\bar{w}_{\alpha 0}\bar{w}_{\alpha 0}'' \\
& -\hat{K}_s\left(\overline{II}_\alpha(1,1)\left(\bar{\psi}_{\alpha 0}\bar{\psi}_{\alpha 0}'\right)' + \overline{II}_\alpha(0,1)\left(\bar{w}_{\alpha 0}\bar{\psi}_{\alpha 0}\right)'\right)\Bigg] - Ck_7\left(\overline{II}_\alpha(0,0)\bar{v}_{\alpha 0} + \overline{II}_\alpha(1,0)\bar{\varphi}_{\alpha 0}'\right)\bar{\psi}_{\alpha 0} \\
& +4C_2\overline{II}_\alpha(0,0)\bar{\varphi}_{\alpha 0}{}^2 - Ck_2\Bigg[\overline{II}_\alpha(0,0)\left(\hat{K}_s\bar{\varphi}_{\alpha 0}\bar{w}_{\alpha 0}' + K_s\left(\left(\bar{w}_{\alpha 0}'\right)^2 + \bar{w}_{\alpha 0}\bar{w}_{\alpha 0}'' + \bar{w}_{\alpha 0}\bar{\varphi}_{\alpha 0}'\right)\right) \\
& +\overline{II}_\alpha(1,0)\left(\hat{K}_s\bar{\varphi}_{\alpha 0}\bar{\psi}_{\alpha 0}' + K_s\left(2\bar{w}_{\alpha 0}'\bar{\psi}_{\alpha 0}' + \bar{w}_{\alpha 0}\bar{\psi}_{\alpha 0}'' + \bar{\psi}_{\alpha 0}\bar{w}_{\alpha 0}'' + \bar{\psi}_{\alpha 0}\bar{\varphi}_{\alpha 0}'\right)\right) \\
& +K_s\overline{II}_\alpha(2,0)\left(\left(\bar{\psi}_{\alpha 0}'\right)^2 + \bar{\psi}_{\alpha 0}\bar{\psi}_{\alpha 0}''\right)\Bigg] - Ck_3\Big[2\overline{II}_\alpha(2,-1)\bar{\psi}_{\alpha 0}\bar{\varphi}_{\alpha 0}' + 2\overline{II}_\alpha(0,-1)\left(\bar{v}_{\alpha 0}+\bar{\psi}_{\alpha 0}\right)\bar{w}_{\alpha 0} \\
& +2\overline{II}_\alpha(1,-1)\left(\bar{w}_{\alpha 0}\bar{\varphi}_{\alpha 0}' + \bar{\psi}_{\alpha 0}{}^2 + \bar{v}_{\alpha 0}\bar{\psi}_{\alpha 0}\right) + 2\overline{II}_\alpha(1,0)\bar{v}_{\alpha 0}\bar{\varphi}_{\alpha 0}' + \overline{II}_\alpha(0,0)\left(\bar{v}_{\alpha 0}{}^2 + \bar{\psi}_{\alpha 0}{}^2\right) \\
& +2\overline{II}_\alpha(2,0)\left(\bar{\varphi}_{\alpha 0}'\right)^2\Big] + Ck_8\Big[\overline{II}_\alpha(2,0)\left(\bar{\psi}_{\alpha 0}'\right)^2 + \overline{II}_\alpha(0,0)\left(\bar{w}_{\alpha 0}'\right)^2\Big] - K_sCk_4\Bigg[\overline{II}_\alpha(1,1)\left(\bar{\varphi}_{\alpha 0}\bar{\varphi}_{\alpha 0}'\right)' \\
& +\overline{II}_\alpha(0,1)\left(\bar{v}_{\alpha 0}\bar{\varphi}_{\alpha 0} + \bar{\varphi}_{\alpha 0}\bar{\psi}_{\alpha 0}\right)'\Bigg] + \hat{K}_s k\Bigg[\overline{II}_\alpha(2,1)\left(\bar{\varphi}_{\alpha 0}'\bar{\psi}_{\alpha 0}'\right)' + \overline{II}_\alpha(1,1)\left(\bar{v}_{\alpha 0}\bar{\psi}_{\alpha 0}' + \bar{\varphi}_{\alpha 0}'\bar{w}_{\alpha 0}'\right)' \\
& +\overline{II}_\alpha(0,1)\left(\bar{v}_{\alpha 0}\bar{w}_{\alpha 0}'\right)'\Bigg] + 2k\Big[\overline{II}_\alpha(2,-2)\bar{\psi}_{\alpha 0}{}^2 + 2\overline{II}_\alpha(1,-2)\bar{w}_{\alpha 0}\bar{\psi}_{\alpha 0} + \overline{II}_\alpha(0,-2)\bar{w}_{\alpha 0}{}^2\Big]
\end{aligned}
\tag{A14}
$$

$$
\begin{aligned}
\left\{\mathbf{F}_{\alpha 1}^{II_\alpha}\right\}_4 = -Ck_1\Bigg[&\overline{II}_\alpha(0,1)\bar{\varphi}_{\alpha 0}\bar{w}_{\alpha 0}' + \hat{K}_s\left(\overline{II}_\alpha(1,1)\bar{w}_{\alpha 0}'' + \overline{II}_\alpha(2,1)\bar{\psi}_{\alpha 0}''\right)\bar{\psi}_{\alpha 0} - \overline{II}_\alpha(1,0)\bar{w}_{\alpha 0}\bar{w}_{\alpha 0}'' \\
& -\overline{II}_\alpha(2,0)\left(\left(\bar{w}_{\alpha 0}\bar{\psi}_{\alpha 0}'\right)' + \bar{\psi}_{\alpha 0}\bar{w}_{\alpha 0}''\right) - \overline{II}_\alpha(3,0)\bar{\psi}_{\alpha 0}\bar{\psi}_{\alpha 0}''\Bigg] - Ck_9\overline{II}_\alpha(1,1)\left(\bar{v}_{\alpha 0}+\bar{\psi}_{\alpha 0}\right)\bar{\varphi}_{\alpha 0}' \\
& -Ck_2\Bigg[\overline{II}_\alpha(1,0)\left(K_s\left(\left(\bar{w}_{\alpha 0}'\right)^2 + \bar{w}_{\alpha 0}\bar{\varphi}_{\alpha 0}' + \bar{w}_{\alpha 0}\bar{w}_{\alpha 0}''\right) + \hat{K}_s\bar{\varphi}_{\alpha 0}\bar{w}_{\alpha 0}'\right) \\
& +\overline{II}_\alpha(2,0)\left(K_s\left(\left(\bar{w}_{\alpha 0}\bar{\psi}_{\alpha 0}'\right)' + \bar{\psi}_{\alpha 0}\bar{w}_{\alpha 0}'' + \bar{\psi}_{\alpha 0}\bar{\varphi}_{\alpha 0}'\right) + \hat{K}_s\bar{\varphi}_{\alpha 0}\bar{w}_{\alpha 0}'\right) \\
& +K_s\overline{II}_\alpha(3,0)\left(\left(\bar{\psi}_{\alpha 0}'\right)^2 + 2\bar{\psi}_{\alpha 0}\bar{\psi}_{\alpha 0}''\right)\Bigg] - Ck_3\Big[\overline{II}_\alpha(3,0)\left(\bar{\varphi}_{\alpha 0}'\right)^2 + \overline{II}_\alpha(0,-1)\bar{w}_{\alpha 0}{}^2 \\
& +2\left(\overline{II}_\alpha(2,-1) + \overline{II}_\alpha(0,1)\right)\bar{v}_{\alpha 0}\bar{\psi}_{\alpha 0} + 2\left(2\overline{II}_\alpha(1,-1) + \overline{II}_\alpha(0,0)\right)\bar{w}_{\alpha 0}\bar{\psi}_{\alpha 0} \\
& +3\left(\overline{II}_\alpha(1,0) + \overline{II}_\alpha(2,-1)\right)\bar{\psi}_{\alpha 0}{}^2 + \left(\overline{II}_\alpha(0,1) + \overline{II}_\alpha(1,0)\right)\bar{v}_{\alpha 0}{}^2 + 2\overline{II}_\alpha(2,0)\bar{v}_{\alpha 0}\bar{\varphi}_{\alpha 0}' \\
& +2\overline{II}_\alpha(1,-1)\bar{v}_{\alpha 0}\bar{w}_{\alpha 0} + 2\overline{II}_\alpha(2,-1)\bar{w}_{\alpha 0}\bar{\varphi}_{\alpha 0}' + 2\overline{II}_\alpha(3,-1)\bar{\psi}_{\alpha 0}\bar{\varphi}_{\alpha 0}' + \overline{II}_\alpha(2,1)\left(\bar{\varphi}_{\alpha 0}'\right)^2\Big] \\
& -Ck_4\Bigg[\overline{II}_\alpha(2,1)\left(\hat{K}_s\left(\bar{\psi}_{\alpha 0}'\right)^2 + K_s\left(\bar{\varphi}_{\alpha 0}\bar{\varphi}_{\alpha 0}'\right)'\right) + K_s\overline{II}_\alpha(1,1)\left(\left(\bar{\varphi}_{\alpha 0}\bar{v}_{\alpha 0}\right)' + \bar{\psi}_{\alpha 0}\bar{\varphi}_{\alpha 0}'\right)\Bigg] \\
& +C_{12}\overline{II}_\alpha(0,1)\left(\hat{K}_s\left(\bar{w}_{\alpha 0}'\right)^2 + K_s\bar{\varphi}_{\alpha 0}\bar{w}_{\alpha 0}'\right) + Ck_8\Big[\overline{II}_\alpha(3,0)\left(\bar{\psi}_{\alpha 0}'\right)^2 + \overline{II}_\alpha(1,0)\left(\bar{w}_{\alpha 0}'\right)^2\Big] \\
& -Ck_7\Big[2\overline{II}_\alpha(2,0)\bar{\psi}_{\alpha 0}\bar{\varphi}_{\alpha 0}' + 2\overline{II}_\alpha(1,0)\left(\bar{v}_{\alpha 0}\bar{\psi}_{\alpha 0} + \bar{w}_{\alpha 0}\bar{\varphi}_{\alpha 0}'\right) + \overline{II}_\alpha(0,0)\bar{v}_{\alpha 0}\bar{w}_{\alpha 0}\Big] + \hat{K}_s k\Big[\overline{II}_\alpha(3,1)\left(\bar{\varphi}_{\alpha 0}'\bar{\psi}_{\alpha 0}'\right)' \\
& +\overline{II}_\alpha(2,1)\left(\left(\bar{\varphi}_{\alpha 0}'\bar{w}_{\alpha 0}'\right)' + \left(\bar{v}_{\alpha 0}\bar{\psi}_{\alpha 0}'\right)'\right) + \overline{II}_\alpha(1,1)\left(\left(\bar{v}_{\alpha 0}\bar{w}_{\alpha 0}'\right)' + \left(\bar{w}_{\alpha 0}' + \bar{\varphi}_{\alpha 0}\right)\bar{\psi}_{\alpha 0}'\right)\Big] \\
& +2k\Big[\overline{II}_\alpha(1,-2)\bar{w}_{\alpha 0}{}^2 + \left(\overline{II}_\alpha(3,-2) + \overline{II}_\alpha(0,1)\right)\bar{\psi}_{\alpha 0}{}^2 + 2\overline{II}_\alpha(2,-2)\bar{w}_{\alpha 0}\bar{\psi}_{\alpha 0}\Big]
\end{aligned}
\tag{A15}
$$

References

[1] M. C. Boyce, E.M. Arruda, Constitutive models of rubber elasticity: a review, *Rubber Chemistry and Technology*, Vol. 73, No. 3, pp. 504-523, 2000.

[2] W. Ma, B. Qu, F. Guan, Effect of the friction coefficient for contact pressure of packer rubber, *Journal of Mechanical Engineering Science,* Vol. 228, No. 16, pp. 2881-2887, 2014.

[3] T. Sussman, K. J. Bathe, A finite element formulation for nonlinear incompressible elastic and inelastic analysis, *Computers & Structures,* Vol. 26, No. 112, pp. 357-109, 1987.

[4] M. Levinson, I. W. Burgess, A comparison of some simple constitutive relations for slightly compressible rubber-like materials, *International Journal of Mechanical Sciences*, Vol. 13, No. 6, pp. 563-572, 1971.

[5] J. C. Simo, R. L. Taylor, Penalty function formulations for incompressible nonlinear elastostatics, *Computer Methods in Applied Mechanics and Engineering*, Vol. 35, pp. 107-118, 1982.

[6] J. C. Simo, R. L. Taylor, Quasi-incompressible finite elasticity in principal stretches. Continuum basis and numerical algorithms, *Computer Methods in Applied Mechanics and Engineering,* Vol. 85, No. 3, pp. 273-310, 1991.

[7] J. S. Chen, C. Pan, A pressure projection method for nearly incompressible rubber hyperelasticity, Part I: Theory, *Journal of Applied Mechanics,* Vol. 63, No. 4, pp. 862-868, 1996.

[8] J. S. Chen, C. T. Eu, C. Pan, A pressure projection method for nearly incompressible rubber hyperelasticity, Part II: Applications, *Journal of Applied Mechanics,* Vol. 63, No. 4, pp. 869-876, 1996.

[9] I. Bijelonja, I. Demirdžic, S. Muzaferija, A finite volume method for large strain analysis of incompressible hyperelastic materials, *International Journal for Numerical methods in Engineering,* Vol. 64, pp. 1594-1609, 2005.

[10] C. A. C. Silva, M. L. Bittencourtb, Structural shape optimization of 3D nearly-incompressible hyperelasticity problems, *Latin American Journal of Solids and Structures*, Vol. 5, pp. 129-156, 2008.

[11] S. Doll, K. Schweizerhof, On the development of volumetric strain energy functions, *Journal of Applied Mechanics,* Vol. 97, pp.17–21, 2000.

[12] H. Ghaemi, K. Behdinan, A. Spence, On the development of compressible pseudo-strain energy density function for elastomers Part 1. Theory and experiment, *Journal of Materials Processing Technology*, Vol. 178, pp. 307-316, 2006.

[13] G. Montella, A. Calabrese, G. Serino, Mechanical characterization of a Tire Derived Material: experiments, hyperelastic modeling and numerical validation, *Construction and Building Materials,* Vol. 66, pp. 336-347, 2014.

[14] V. Dias, C. Odenbreit, O. Hechler, F. Scholzen, T. B. Zineb, Development of a constitutive hyperelastic material law for numerical simulations of adhesive steel–glass connections using structural silicone, *International Journal of Adhesion and Adhesives,* Vol. 48, pp. 194–209, 2014.

[15] Y. Zhu, X. Y. Luo, R. W. Ogden, Nonlinear axisymmetric deformations of an elastic tube under external pressure, *European Journal of Mechanics-A/Solids*, Vol. 29, No. 2, pp. 216-229, 2010.

[16] M. Tanveer, J. W. Zu, Non-linear vibration of hyperelastic axisymmetric solids by a mixed p-type method, *International Journal of Non-Linear Mechanics,* Vol. 47, pp. 30-41, 2012.

[17] J. Kiendl, M. C. Hsu, M. C. H. Wu, A. Reali, Isogeometric Kirchhoff–Love shell formulations for general hyperelastic materials. *Computer Methods in Applied Mechanics and Engineering.,* Vol. 291, pp. 280-303, 2015.

[18] H. R. Eipakchi, Third-order shear deformation theory for stress analysis of a thick conical shell under pressure, *Journal of Mechanics of materials and structures*, Vol. 5, No. 1, 1-17, 2010.

[19] M. Ghannad, G. H. Rahimi, M. Z. Nejad, Elastic analysis of pressurized thick cylindrical shells with variable thickness made of functionally graded materials, *Composites: Part B,* Vol. 45, pp. 388-396, 2013.

[20] M. Jabbari, M. Z. Nejad, M. Ghannad, Thermo-elastic analysis of axially functionally graded rotating thick truncated conical shells with varying thickness, *Composites: Part B,* Vol. 96, pp. 20-34, 2016.

[21] H. Gharooni, M. Ghannad, M. Z. Nejad, Thermo-elastic analysis of clamped-clamped thick FGM cylinders by using third-order shear deformation theory, *Latin American Journal of Solids and Structures,* Vol. 13, No. 4, pp. 750-774, 2016.

[22] J. Vossoughi, A. Tozeren, Determination of an effective shear modulus of aorta, *Russian Journal of Biomechanics*, Vol. 1-2, pp. 20-36, 1998.

[23] T. E. Carew, R. N. Vaishnav, D. J. Patel, Compressibility of the arterial wall, *Circulation Research,* Vol. 23, No. 1, pp. 61–68, 1968.

[24] K. L. Dorrington, N. G. McCrum, Elastin as a rubber, *Biopolymers*, Vol. 16, No. 6, pp. 1201-1222, 1977.

[25] L. A. Mihai, A. Goriely, How to characterize a nonlinear elastic material? A review on nonlinear constitutive parameters in isotropic finite elasticity, *Journal of Royal Society A,* Vol. 473, No. 2207, 20170607, 2017.

[26] J. D. Humphrey, S. L. O'Rourke, 2015, *An Introduction to Biomechanics Solids and Fluids, Analysis and Design, 2nd ed.,* Springer, New York.

[27] D. Azar, D. Ohadi, A. Rachev, J. F. Eberth, M. J. Uline, T. Shazly, Mechanical and geometrical determinants of wall stress in abdominal aortic aneurysms: A computational study, *PLoS ONE*, Vol. 13, No. 2, e0192032, 2018.

[28] J. N. Reddy, 2002, *Energy principles and variational methods in applied mechanics*, Wiley, New York.

[29] J. T. Oden, A theory of penalty methods for finite element approximations of highly nonlinear problems in continuum mechanics, *Computers and Structures,* Vol. 8, pp. 445-449, 1978.

[30] G. A. Holzapfel, 2000, *Nonlinear Solid Mechanics, a Continuum Approach for Engineering*, Wiley, New York.

[31] Y. Başar, D. Weichert, 2000, *Nonlinear Continuum Mechanics of Solids*, Springer, Berlin.

[32] I. Doghri, 2000, *Mechanics of Deformable Solids: Linear, Nonlinear, Analytical and Computational Aspects*, Springer, Berlin.

[33] J. N. Reddy, 2004, *Mechanics of Laminated Composite Plates and Shells: Theory and Analysis, 2nd ed.,* CRC Press, New York.

[34] A. H. Nayfeh, 1981, *Introduction to Perturbation Techniques,* Wiley, New York.

[35] Y. Payan, J. Ohayon, (Eds.) 2017, *Biomechanics of Living Organs: Hyperelastic Constitutive Laws for Finite Element Modeling,* World Bank Publications, London.

[36] G. A. Holzapfel, R. W. Ogden, (Eds.) 2003, *Biomechanics of soft tissue in cardiovascular systems,* Springer-Verlag, Austria.

[37] J. H. Kim, S. Avril, A. Duprey, J. P. Favre, Experimental characterization of rupture in human aortic aneurysms using full-field measurement technique, *Biomechanics and Modeling in Mechanobiology*, Vol. 11, No. 6, pp. 841-854, 2012.

[38] G. A. Holzapfel, T. C. Gasser, Computational stress–deformation analysis of arterial walls including high-pressure response *International Journal of Cardiology,* Vol. 116, pp. 78-85, 2007.

[39] R. Mihara, A. Takasu, K. Maemura, T. Minami, Prolonged severe hemorrhagic shock at a mean arterial pressure of 40 mmHg does not lead to brain damage in rats, *Acute Medicine & Surgery*, Vol. 5, pp. 350-357, 2018.

[40] M. Cecconi, D. D. Backer, M. Antonelli, R. Beale, J. Bakker, C. Hofer, R. Jaeschke, A. Mebazaa, M. R. Pinsky, J. L. Teboul, J. L. Vincent, A. Rhodes, Consensus on circulatory shock and hemodynamic monitoring. Task force of the European Society of Intensive Care Medicine, *Intensive Care Medicine*, Vol. 40, pp. 1795-1815, 2014.

[41] B. R. Simon, M. V. Kaufmann, M. A. McAfee, A. L. Baldwin, L. M. Wilson, Identification and determination of material properties for porohyperelastic analysis of large arteries, *Journal of Biomechanical Engineering*, Vol. 120, No. 2, pp. 188-194, 1998.